

1 **Murine blastocysts generated by in vitro fertilization show increased Warburg metabolism**
2 **and altered lactate production**

3

4 Seok Hee Lee ¹, Xiaowei Liu ¹, David Jimenez-Morales ², Paolo F. Rinaudo ^{1,*}

5 ¹ Center for Reproductive Sciences, Department of Obstetrics and Gynecology, University of
6 California San Francisco, San Francisco, CA 94143, U.S.A

7 ² Division of Cardiovascular Medicine, Department of Medicine, Stanford University, Stanford,
8 CA, USA.

9 * Correspondence: paolo.rinaudo@ucsf.edu

10	ART	Assisted reproductive technologies
11	ATP	Adenosine triphosphate
12	CMF2HC	4-chloromethyl- 6,8- difluoro-7-hydroxycoumarin
13	COCs	Cumulus-oocyte complexes
14	DCF	Dichlorodihydrofluorescein
15	DNPH	2,4-Dinitrophenylhydrazine
16	ECAR	Extracellular acidification rate
17	FB	Flushed blastocyst
18	FCCP	Carbonyl cyanide-4-trifluoromethoxyphenylhydrazone
19	GSH	Glutathione
20	hCG	Human chorionic gonadotropin
21	HTF	Human tubal fluid
22	H2DCFDA	2',7'-dichlorodihydro-fluorescein diacetate
23	IVC	In vitro cultivation
24	IVF	In vitro fertilization
25	KSOM	Potassium simplex optimization medium
26	LDHA	Lactate dehydrogenase A
27	LDHB	Lactate dehydrogenase B
28	MCT1	Monocarboxylate transporter 1
29	MPA	Metaphosphoric acid
30	NAD	Nicotinamide adenine dinucleotide
31	OCR	Oxygen consumption rate
32	PBS	Phosphate buffer saline
33	PER	Proton efflux rate
34	PGF2	Prostaglandin F2
35	PMSG	Pregnant mare serum gonadotrophin
36	PPP	Pentose phosphate pathway
37	PVA	Poly vinyl alcohol
38	ROS	Reactive oxygen species

39	TCA	Tricarboxylic cycle
40	2-DG	2-deoxy-D-glucose
41	8-OHdG	8-Hydroxyguanosine

Abstract

In vitro fertilization (IVF) has resulted in the birth of over 8 million children. Although most of IVF-conceived children are healthy, several studies suggest an increased risk of altered growth rate, cardiovascular dysfunction, and glucose intolerance in this population compared to naturally conceived children. However, a clear understanding of how embryonic metabolism is affected by culture condition and how embryos reprogram their metabolism is unknown.

Here, we studied oxidative stress and metabolic alteration in blastocysts conceived by natural mating or by IVF and culture in physiologic (5%) or atmospheric (20%) oxygen. We found that IVF-generated blastocyst manifest increased reactive oxygen species, oxidative damage to DNA/lipid/proteins, and reduction in glutathione. Metabolic analysis revealed IVF-generated blastocysts display decreased mitochondria respiration and increased glycolytic activity suggestive of enhanced Warburg metabolism. These findings were corroborated by altered intracellular and extracellular pH and increased intracellular lactate levels in IVF-generated embryos. Comprehensive proteomic analysis and targeted immunofluorescence showed reduction of LDH-B and MCT1, enzymes involved in lactate metabolism. Importantly, these enzymes remained downregulated in tissues of adult IVF-conceived mice, suggesting that metabolic alterations in IVF-generated embryos may result in alteration in lactate metabolism. These findings suggest that alterations in lactate metabolism is a likely mechanism involved in genomic reprogramming and could be involved in the developmental origin of health and disease.

1. Introduction

Assisted reproductive technologies (ART), including in vitro fertilization (IVF) show excellent success resulting in the birth of over 8 million children worldwide (Berntsen 2019). While the great majority of children born with these technologies are healthy, it has also been suggested that ARTs could be associated with an increased risk of adverse perinatal outcome and possibly, an increased predisposition to adult-onset chronic diseases (Berntsen 2019; Kleijkers 2014; Qin 2017). In particular, several reports have shown that ART offspring display altered growth pattern (Ceelen 2009; Kleijkers 2016), increased risk of cardiometabolic dysfunction (Ceelen 2008; Guo 2017), higher systolic and diastolic blood pressures (Cui 2021; Guo 2017; Meister 2018), premature vascular aging (Meister 2018), altered lipid metabolism (Guo 2017), and increased the prevalence of cerebral palsy (Goldsmith 2018). Therefore, assessing the health of ART offspring and understanding the safety of ART is of critical importance.

Importantly, different culture media and oxygen concentration may result in different stress to the embryo (Chronopoulou 2015; Feuer 2016; Rinaudo 2004; Rinaudo 2006b) with possible subsequent alterations in health of the individual. In particular, either 5% (physiologic) or 20% oxygen (atmospheric) concentrations have been widely used in clinical settings and in 2014 only 25% of 265 IVF clinics reported of using 5% oxygen for culture of human embryos (Christianson 2014). This is relevant, since it is well known that environmental oxygen can influence embryo development and their intracellular redox balance (Bavister, 2004; Rinaudo 2006b). Overall, low oxygen tension can significantly improve the cleavage rate, implantation, pregnancy and birth rates in humans compared with an atmosphere condition (Adam 2004; Bavister, 2004; Ciray 2009; Ma 2017; Meintjes 2009; Preis 2007; Waldenstrom 2009). Supra physiological oxygen concentration result in increase in reactive oxygen species (ROS) (Ryan 1998) and likely result in oxidative damage and metabolic alterations to embryos.

Despite investigations (Gardner 2013), it is unknown how metabolism is reprogrammed in early embryos following culture ex vivo. This is a critical question, since metabolic alterations occurring during embryo development will likely be responsible for epigenetic reprogramming; therefore, understanding these metabolic alterations might provide an initial window into what ultimately will determine individual's health (Tzika 2018). Preimplantation embryo metabolism is unique and different from somatic cells. The Krebs cycle is the main source of energy throughout the preimplantation period. Glycolysis is slowly utilized during the first 1-2 days of development but both an increase in glycolysis and oxygen consumption (via mitochondria) is notable at the blastocyst stage (Leese, 2012). Importantly, preimplantation embryos show an accentuation of the Warburg metabolism (Warburg, 1956), i.e. higher production of ATP through glycolysis and increased conversion of pyruvate into lactate, even in the presence of oxygen (Redel 2011). This process is facilitated by the lactate dehydrogenase class of enzymes (LDH-A and LDH-B) (Redel 2011).

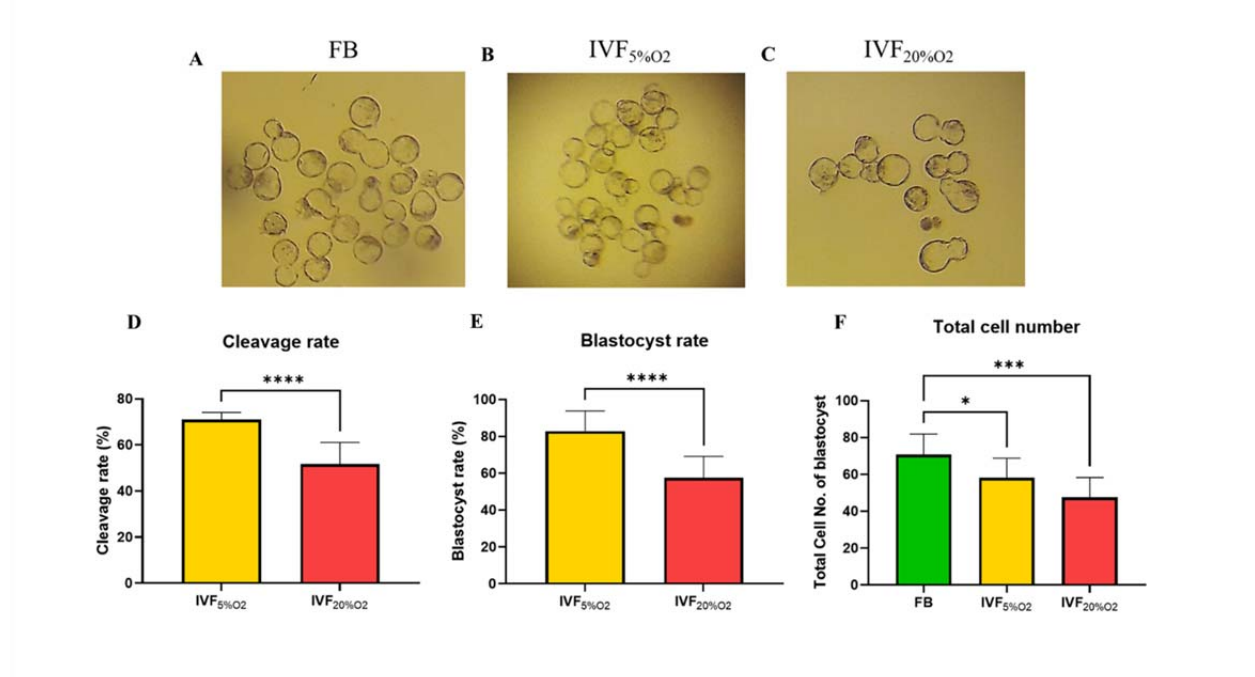
Given result to date we sought to obtain a clearer understanding of embryonic metabolism in mouse embryos generated in vivo or in vitro. Blastocysts generated in vivo after mating were used as a control (Flushed blastocyst group or FB). Two experimental groups were used: embryos generated by IVF and cultured to the blastocyst stage in optimal conditions using KSOM medium with amino acids and 5% oxygen concentration (IVF 5% or optimal conditions group) or 20% oxygen concentration (IVF 20% or suboptimal conditions group). These groups of embryos were compared for: 1) oxidative stress, (including ROS levels, markers of oxidative damage to embryos, GSH level), 2) changes in mitochondria/glycolytic function using the Agilent Seahorse XF HS Mini Analyzer and measuring selected metabolites (lactate and pyruvate) and embryonic pH; and 3) comprehensive proteomic analysis.

108 We found that embryos generated by IVF show profound alterations in metabolism. These
109 findings provide a mechanistic insight that link culture conditions to metabolic states and might
110 be useful to select embryos with greater viability.

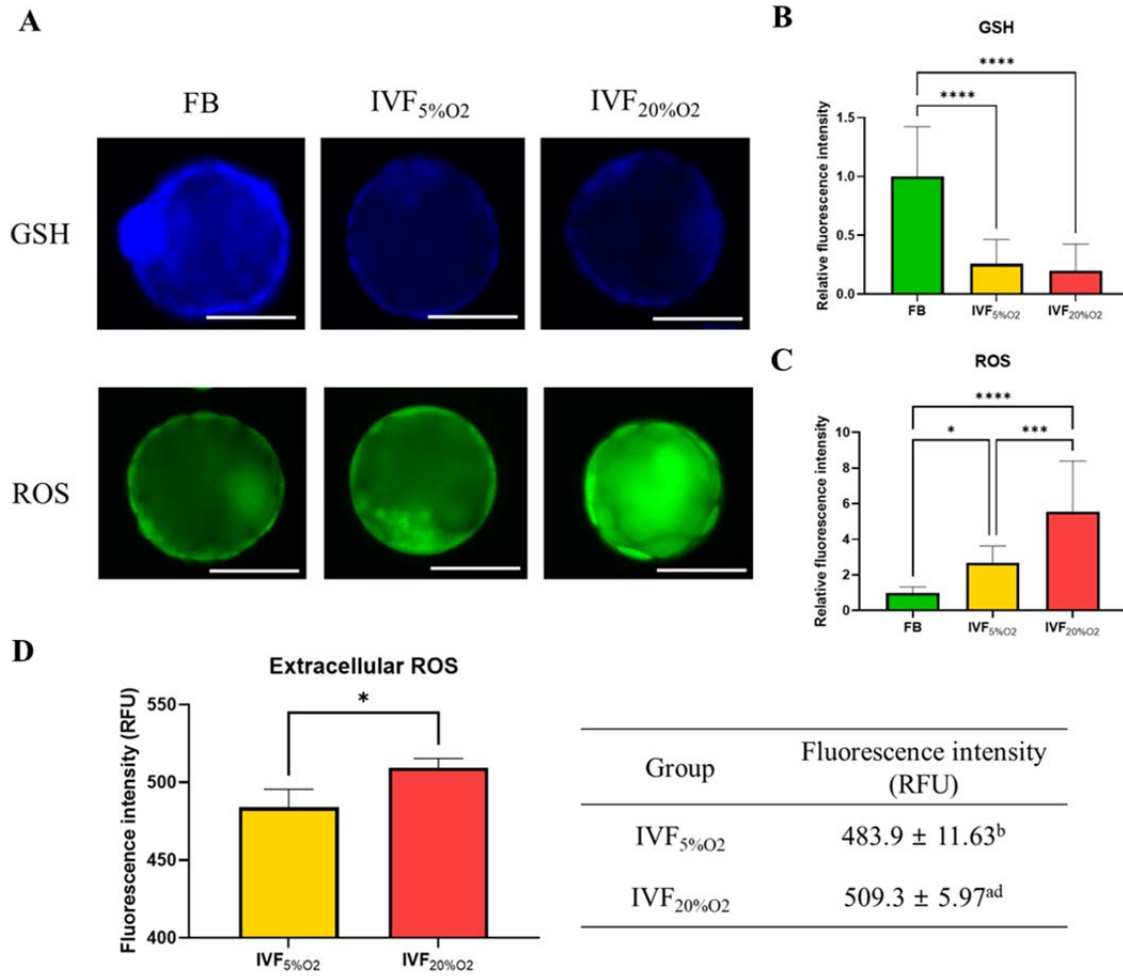
2. Results

2.1. Embryo generated by IVF show similar morphology but lower development to the blastocyst stage and increased in ROS and oxidative damage

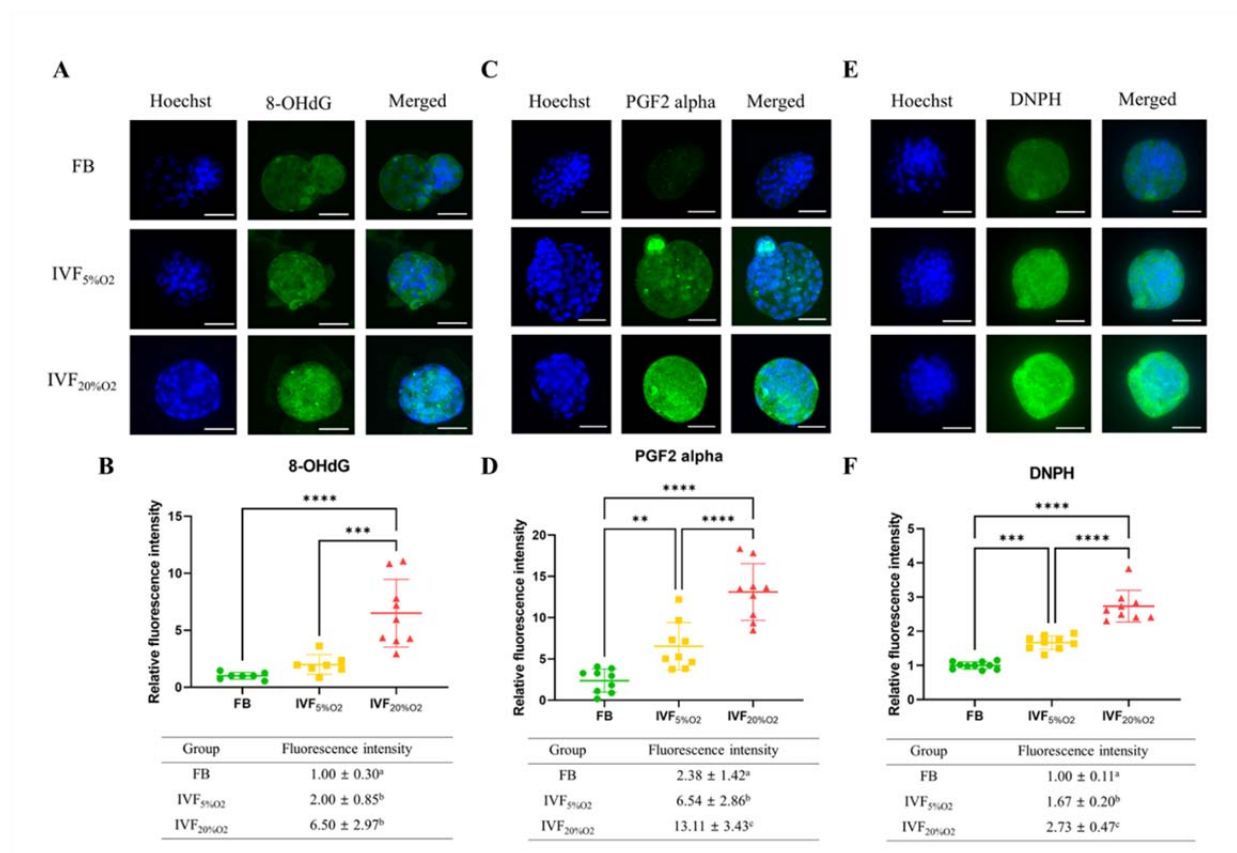
Only expanded blastocysts of similar morphology were used for all experiments (Supplemental Figure 1A-C). Overall, IVF-generated embryos showed lower development if cultured with atmospheric oxygen (Supplemental Figure 1D, E). IVF generated blastocysts had lower total cell number, compared to in vivo generated blastocysts (Supplemental Figure 1F). These morphologic and developmental changes were mirrored by increase in oxidative stress in IVF-conceived embryos, with embryos exposed to 20% O₂ (IVF 20%O₂) showing higher oxidative stress.



In particular, IVF-generated blastocysts had significantly decreased level of GSH compared to in vivo blastocysts (Figure 1A, B), increase in intracellular ROS (Figure 1C) and extracellular ROS levels (Figure 1D).



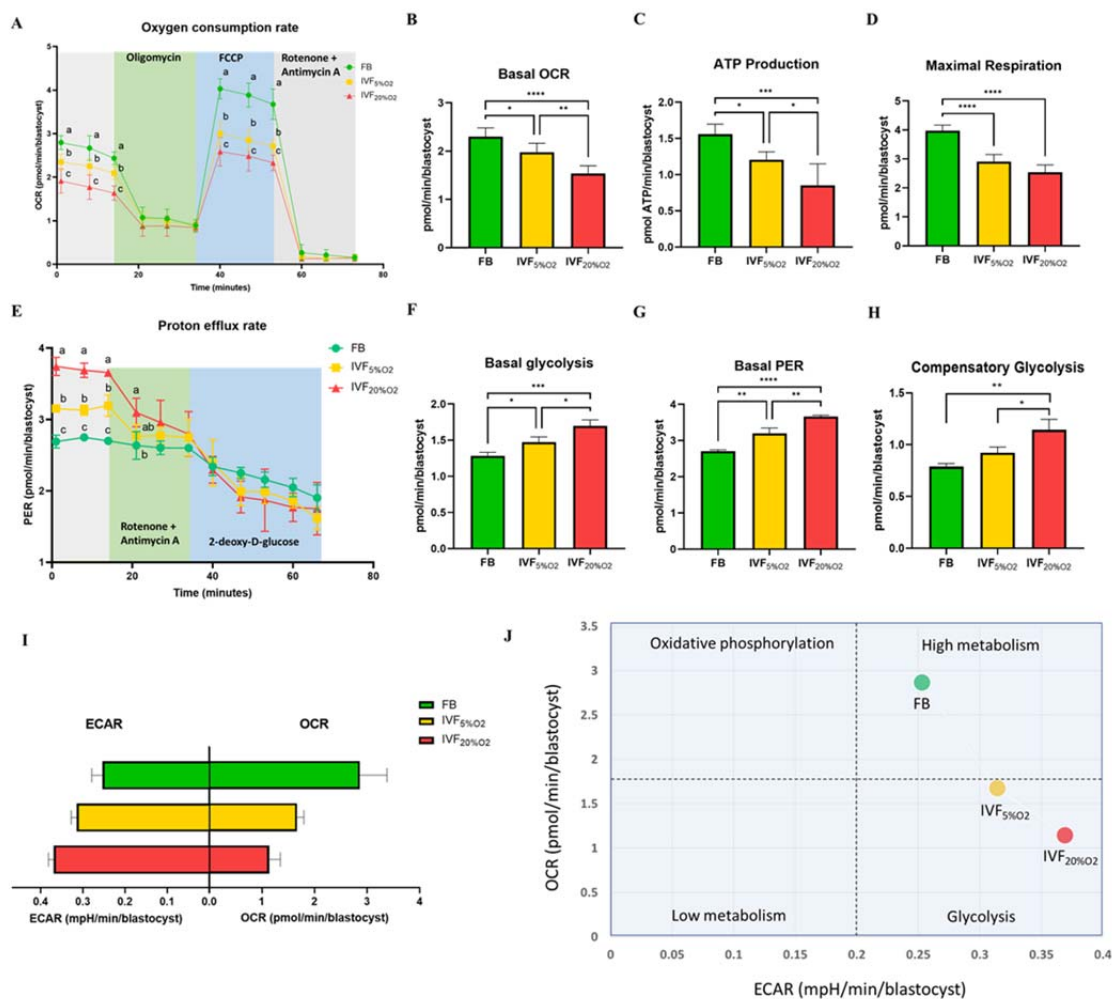
126
 127 Importantly, IVF-generated embryos showed increased in oxidative damage to DNA (intensity of
 128 8-OHdG, Figure 2A, B), lipids (PGF2-alpha, Figure 2C, D) and proteins (levels of DNPH,
 129 Figure 2E, F).



2.2. IVF generated blastocysts showed decreased mitochondrial activity and increased glycolytic function, indicative of increase Warburg metabolism

We (Belli 2019) and others (Acton 2004; Ren 2015) have shown that IVF-generated blastocysts show an increase in mitochondrial alterations. To evaluate the physiological consequences of increase in oxidative stress to embryos, mitochondrial metabolism (oxygen consumption rate OCR) and glycolysis (proton efflux rate, PER; extracellular acidification rate, ECAR) were assessed using the Agilent Seahorse XF HS Mini (Figure 3). IVF-derived blastocysts showed significantly lower basal steady-state OCR (Figure 3A, B), ATP production (Figure 3C) and maximal respiration (Figure 3D), compared to in vivo-conceived control. Overall, these effects were accentuated in embryos cultured in atmospheric oxygen (IVF20%O₂ group).

Analysis of glycolytic function revealed that IVF-generated embryos showed higher basal glycolysis (Figure 3E, F), basal proton efflux rate (PER, Figure 3G) and higher compensatory glycolysis (Figure 3H) compared to the FB group. Culture under atmospheric oxygen (IVF20% group) resulted in significantly increase in glycolysis. Overall, these results show that IVF-generated embryos favor glycolysis over oxidative phosphorylation (Figure 3I, J), indicating an accentuation of Warburg metabolism.



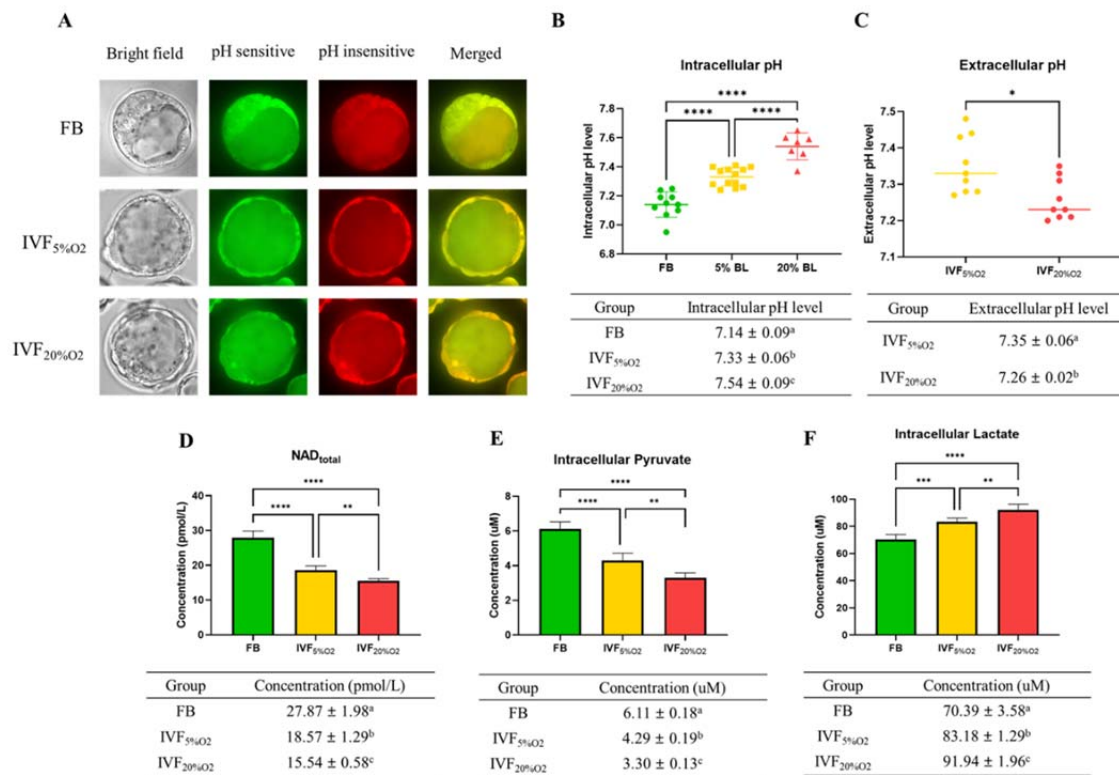
2.3. IVF-generated embryos show alterations of Intracellular/extracellular pH, NAD, lactate and pyruvate levels

To gain a more detailed understanding of metabolic alterations occurring in IVF embryos we measured pH and selected metabolites levels. IVF-generated blastocysts had significantly higher intracellular pH (Figure 4A, B), while extracellular pH level was lower and showed an inverse correlation to intracellular pH (Figure 4C).

NAD levels were significantly lower in IVF-generated embryos (Figure 4D) compared to FB group.

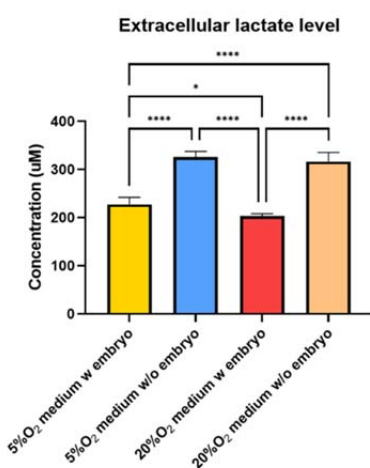
Next, we measured intracellular pyruvate and lactate levels, the final metabolites of glycolysis.

Intracellular pyruvate levels were decreased (Figure 4E), while intracellular lactate levels were increased (Figure 4F) in IVF-generated embryos compared to in vivo embryos.



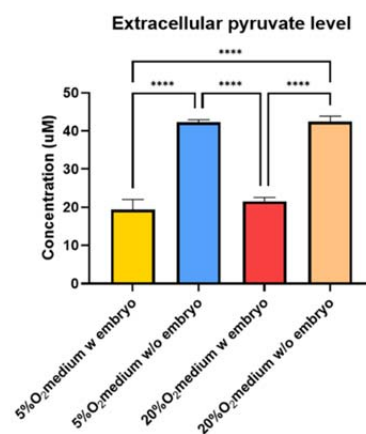
Extracellular lactate and pyruvate levels were decreased in culture media of IVF embryos (Supplemental Figure 2A, B).

A



Group	Concentration (uM)
5%O ₂ medium w embryo	227.6 ± 14.53 ^a
5%O ₂ medium w/o embryo	325.5 ± 12.02 ^b
20%O ₂ medium w embryo	202.9 ± 5.39 ^c
20%O ₂ medium w/o embryo	316.5 ± 19.01 ^{bd}

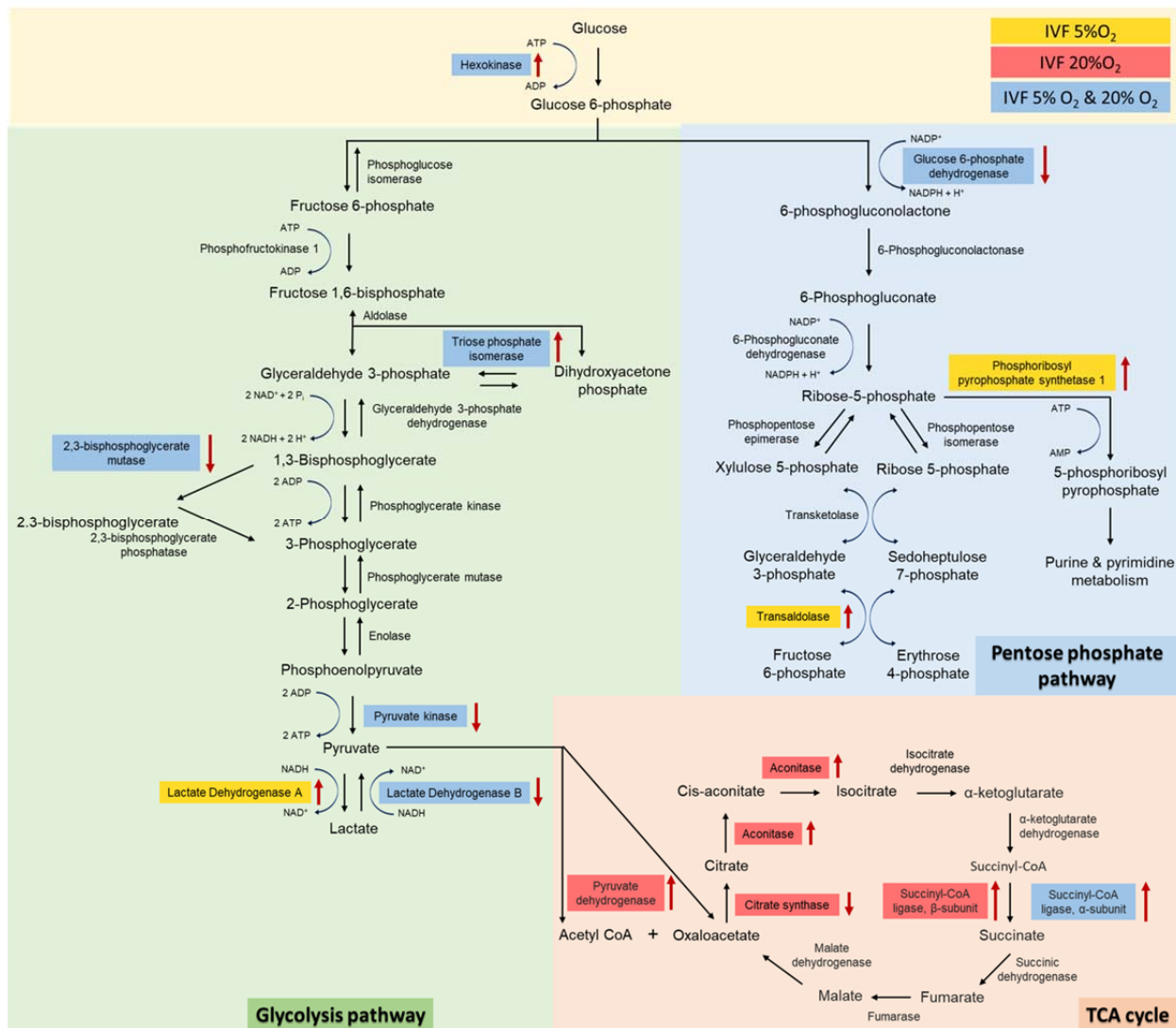
B



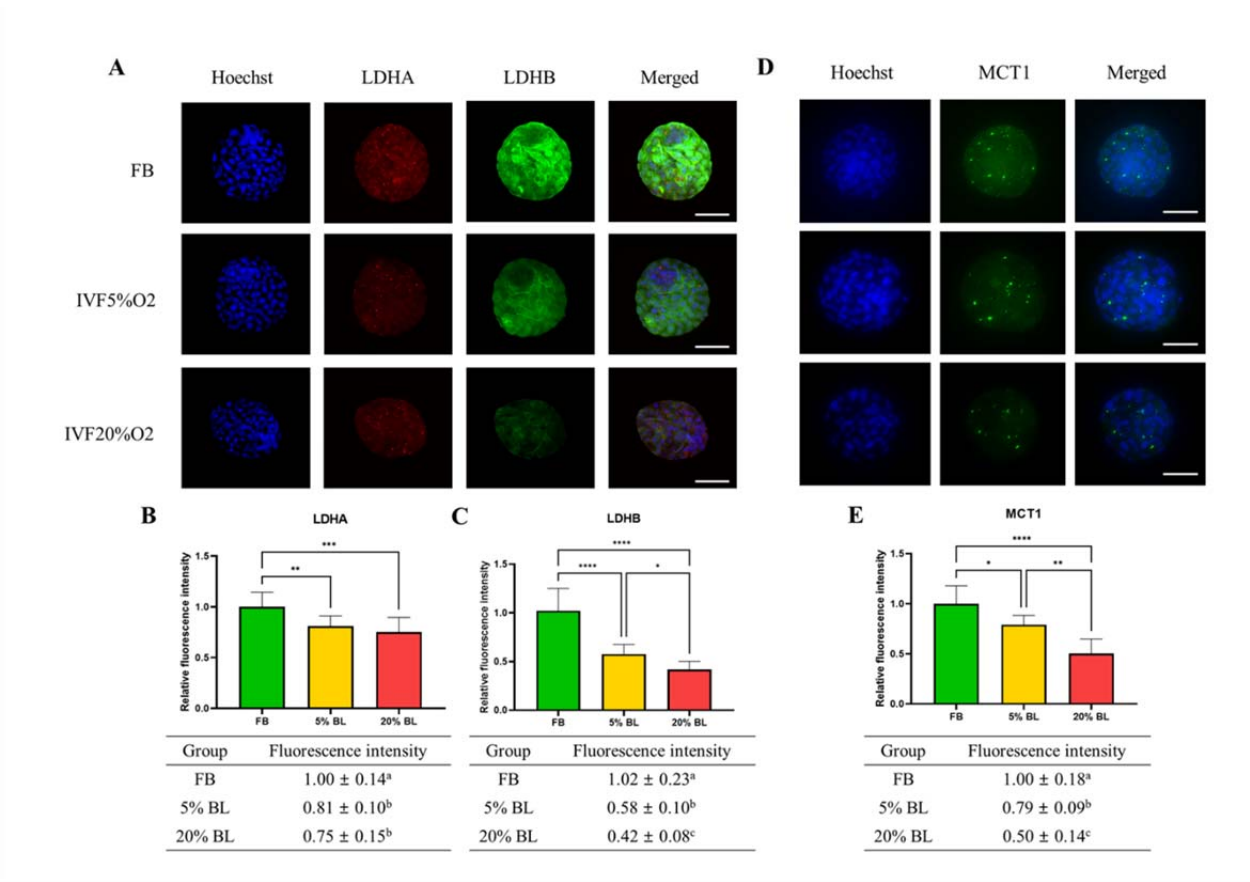
Group	Concentration (uM)
5%O ₂ medium w embryo	19.41 ± 2.64 ^a
5%O ₂ medium w/o embryo	42.28 ± 0.64 ^b
20%O ₂ medium w embryo	21.52 ± 1.07 ^{ac}
20%O ₂ medium w/o embryo	42.49 ± 1.36 ^{bd}

2.4. IVF-generated embryos show alteration in enzymes involved in lactate metabolism

Given the critical role of lactate in metabolism (Brooks, 2020) we performed both an unsupervised analysis of the blastocyst proteome and analyzed key enzymes involved in lactate metabolism. Proteomic analysis revealed that multiple proteins involved in glycolysis (n=5 proteins), pentose phosphate pathway (PPP, n= 3 proteins) and tricarboxylic cycle (TCA, n= 6 proteins) were altered in IVF-generated embryos (Figure 5). Regarding glycolytic proteins, hexokinase 2 and triosephosphate isomerase 1 were upregulated, while 2,3-bisphosphoglycerate mutase, pyruvate kinase, and LDH-B were downregulated in both IVF groups compared to in vivo generated blastocysts. In addition, LDH-A isoenzyme (that favors conversion of pyruvate to lactate (Markert 1975) was upregulated only in IVF5%O₂ blastocysts compared to control.

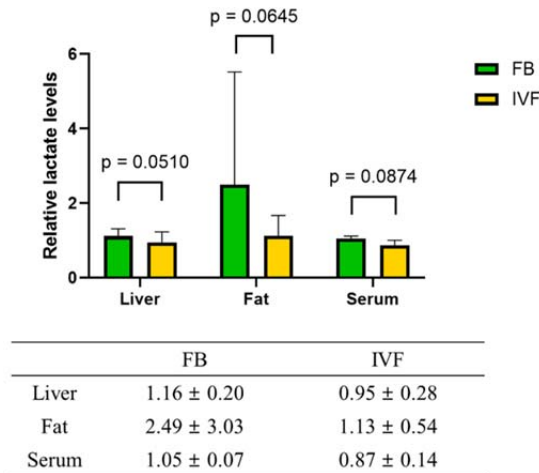


To gain a further understanding of the etiology of altered lactate levels in IVF-generated embryos, we further measured lactate dehydrogenase (LDH-A and LDH-B) and the level of monocarboxylate transporter MCT1 protein (involved in transport of lactate through the plasma and inner mitochondrial membrane) by immunofluorescence (Figure 6). Both LDH isoenzymes were reduced in IVF-generated embryos (Figure 6A-C) compared to in vivo embryos. Similarly, the levels of the transmembrane lactate transporter MCT1 were decreased in IVF embryos compared with FB group (Figure 6D, E).

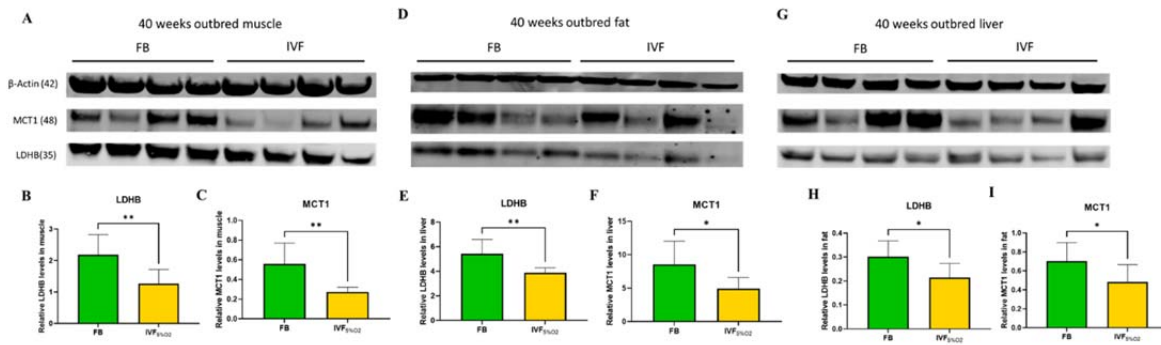


2.5. Several tissues of IVF-generated mice show downregulation of LDH-B and MCT1 proteins

We (Donjacour 2014; Feuer 2014a) and others (Ceelen, 2008, Chen, 2014) have shown that IVF offspring, compared to naturally conceived controls, manifest glucose intolerance and several metabolic alterations (Feuer 2014a). Re-analysis of our past metabolomic data showed a trend for lower lactate in liver ($p=0.05$), fat ($p=0.06$) and serum ($p=0.08$) of IVF5%O₂ conceived mice compared to control (Feuer 2014a) (Supplemental Figure 3).



These findings, together with the reduced levels of LDH-B and MCT1 in IVF embryos prompted us to measure the same enzymes in tissue of adult mice. We found that IVF conceived mice have reduced levels of LDHB (that converts lactate into pyruvate) and MCT1 (involved in transport of lactate through the plasma membrane) proteins in gastrocnemius (Figure 7A-C), fat tissue (Figure 7D-F), and liver (Figure 7G-I).. These data suggest that alteration in lactate metabolism may represent a hallmark of altered metabolic function in ART offspring



3. Discussion

This study reports numerous effects of IVF and embryo culture that will be discussed sequentially: 1) mouse blastocysts generated by IVF show increased in ROS production, subsequent oxidative damage and a plethora of metabolic alterations, 2) oxidative to glycolytic metabolic shift owing to decreased mitochondrial functions and compensatory changes in glycolysis, altered expression of lactate shuttle proteins including LDH and MCT1, and 3) changes in cell redox status and pH, and 4) long-term metabolic dysregulation in IVF animals. In IVF-generated embryos. Importantly, when atmospheric oxygen was used to culture embryos, the phenotype further worsened.

While several studies have suggested an increase in ROS and alteration of antioxidant balance in IVF-generated embryos (Cebal 2007; Goto 1993; Martin-Romero 2008), this study also shows increased oxidative damage to embryos. ROS are second messengers with a likely tight therapeutic window. In fact, during embryo development from the 2-cell to the blastocyst stage, the levels of ROS are increased to maintain their metabolic process (Ryan 1998). However, excessive ROS levels causes a lower oocyte maturation during in vitro maturation and lower embryonic development (Johnson 1994; Luvoni 1996) in addition to cellular apoptosis, DNA damage, inhibition of DNA synthesis, lipid peroxidation, and oxidative modification of proteins (Gardner 1991; Van Blerkom, 2011).

The fact that IVF-generated embryos show altered Redox imbalance is also shown by their reduced level of glutathione, since GSH is one of the main non-enzymatic defenses against ROS in mammalian embryo (Rizzo 2012; Takahashi 1993). The combination of increased ROS and reduced GSH is likely responsible for the increased oxidative damage to DNA, lipid and protein observed in IVF embryos.

Of note, the 8-OHdG is a sensitive indicator of DNA damage and high 8-OHdG levels were detected in patients with low fertilization rates and low blastocyst development (Nishihara 2018). The 8-epi-prostaglandin F2- α (PGF2 α , F2-isoprostane) and 2,4-dinitrophenylhydrazine (DNPH) are widely regarded as specific and stable oxidative stress indicators to measure the degree of lipid peroxidation and protein oxidation respectively (Gongadashetti 2021; Halliwell 2010; Keller 1993; McKinney 2000; Montuschi 2003; Psathakis 2004).

The second important finding of this paper is the alteration in mitochondria and glycolytic function of IVF-generated embryos. That IVF embryos have reduced OCR rate is not surprising, given that we (Belli 2019) and others (Marei 2019) have shown alteration in mitochondria morphology and mitochondrial membrane potential. The current analysis further adds to the knowledge by showing that IVF embryos have reduced ATP production via mitochondrial respiration and show a compensatory increase in glycolysis (Figure 3). The increase is particularly evident in the IVF20%O₂ embryos, that appear to further need to generate energy via glycolysis even when supraphysiologic oxygen is present. Previous studies have shown that the glycolytic rate (percentage of glucose converted to lactate) for mouse blastocysts flushed from the uterus is less than 40%, whereas it increases to over 75% after 3 h of in-vitro culture. This is important, since higher glycolytic rate was associated with lower implantation rates (Lane 1996, 1998) and indeed our past experiments have shown that mouse embryos generated by IVF have lower live birth rate compared to embryos generated in vivo (Xiao Z 2020).

Hence, it appears that vitro-derived blastocysts increase glycolysis to overcome their impaired mitochondrial function. In future observations, linking glucose consumption, lactate ion and proton efflux rates to embryo viability may be useful as predictors of human embryo viability in ART laboratories.

Among the additional metabolic alterations found in IVF-generated embryos, the reduction in NAD levels and increase in intracellular pH are very relevant.

NAD is an essential coenzyme and an obligate cofactor for the catabolism of metabolic fuels in all cell types (Frederick 2016). Growing evidence has confirmed that NAD controls diverse cell signaling pathways (Yamaguchi 2017; Yang 2016). Importantly, age-related reductions in NAD concentration were linked to declining oocyte quality and infertility, and restoration of NAD levels is advocated for the treatment of age-related infertility (Bertoldo 2020). The findings of reduced NAD levels in IVF-derived embryos confirm their significant alteration in energy metabolism and open the possibility that culture media supplemented with NAD might help to overcome their impaired energy metabolism.

The increase in intracellular pH and decreased in extracellular pH found in IVF-generated embryos is particularly important, because it confirms the profound alteration in embryo metabolism. In fact, cancer cells are known to have higher intracellular pH and lower extracellular pH (Webb 2011) and regulation of intra- and extracellular pH is considered essential for cellular physiological and metabolic function (Becker 2021).

Monocarboxylate transporter imbedded in plasma and other cell membranes are symporters moving monocarboxylate anions (e.g., lactate) and protons in a stoichiometric (1:1) ratio. Not surprisingly there is a well-known correlation between intracellular and extracellular pH: while extracellular pH affects intracellular pH (Edwards 1998b), if the embryos produces excess of metabolic acids (either in the form of lactate, protons, or CO₂), extracellular acidification occurs (Gatenby 2008; Gillies 2012; Parks 2011). The existence of this correlation is particularly valuable because precise measurement of extracellular pH could provide insight into the embryonic metabolism and offer diagnostic opportunities to identify healthy embryos. Given that individual blastocysts show variation in intracellular pH, oxidative damage, ROS, NAD levels, and based

on the Goldilocks principle of embryo health (Leese 2016), embryo showing less stress could be identified and selected for early transfer.

We next found that IVF-generated embryos showed decrease in pyruvate and increase in lactate levels. Pyruvate and lactate are key energy sources for the preimplantation embryo. Pyruvate is the preferred energy substrate during the cleavage stage, while glucose consumption is low but tends to increase at the blastocyst stage, when also oxidative phosphorylation increases (Leese 2016). Importantly, while lactate was once believed to be a waste product of anaerobic metabolism, it is now clear that it plays a key role in physiology and metabolism (Brooks, 2018). Lactate is continuously produced under aerobic conditions and plays 3 major roles: 1) it is a major energy source, 2) the most important gluconeogenic precursor, and 3) functions as a signaling molecule. Notably, the product of glycolysis is lactate, not pyruvate (Rogatzki 2015) and lactate oxidation is dominant in vivo. For example, muscle lactate concentration exceeds that of pyruvate by one (10x) to two (200-400x) orders of magnitude in resting and exercising human muscles, respectively (Henderson 2004). Our findings confirm that lactate concentration is 10-fold higher than the lactate concentration, but IVF embryos show a further increase in lactate production since the lactate to pyruvate ratio is 11 for FB embryos, 19 for IVF5%O₂ and 27 for IVF20%O₂. We can therefore hypothesize that the increased level of intracellular lactate in IVF embryos might be a strategy adopted by the embryo to survive the suboptimal culture environment.

The next studies aimed to clarify the molecular mechanism leading to increase lactate levels in IVF embryos. Unsupervised global proteomics analysis revealed that LDH-B was downregulated in IVF embryos. We confirmed these results by performing immunofluorescence studies and found that IVF embryos showed downregulation of both LDHA and B and of the

monocarboxylate transporter, MCT 1, providing an explanation for the increase in their lactate levels. LDH is a tetramer composed of 2 subunits (LDH-M, found in muscles and LDH-H, found in heart), encoded by the LDHA and LDHB genes, that catalyzes the reversible conversion of pyruvate to lactate using NAD as a cofactor (Markert 1975). Lactate production is associated with increase in NAD^+ (Shibata 2021). Importantly, although different isozymes possess different activities (Summermatter 2013), the reduction in protein levels of both isozymes in IVF embryos suggest that LDH is a critical nodus or regulation.

Both LDH-A and B isoenzymes are active in the preimplantation mouse embryos, but LDH-B is the principal form. LDH-A will become predominant at the time of implantation (Auerbach 1967; Lane 2000). Human studies suggest a similar pattern: the mRNA of LDH-B was detected in human oocytes, 4- and 8-cell embryos, while the mRNA for LDH-A was detected only in two of four oocytes and one of three 8-cell embryos. However, the mRNA for testis-specific LDH-C was not detected (Li 2006).

MCT1 is the major transporter for lactate and belongs to a family of proteins involved in the transport of monocarboxylates, such as lactate, pyruvate, and ketone bodies, across the plasma membranes. MCT1 is a proton-linked transporter i.e., it ensures symport of monocarboxylates and protons in a 1: 1 ratio (Chatel 2017). Its downregulation further explains the profound alteration in lactate metabolism in IVF embryos.

Finally, we found that tissues of adult mice conceived by IVF also showed reduced levels of LDH-B and MCT1 proteins in gastrocnemius, fat tissue, and liver and had a trend for lower lactate levels (Supplemental Figure 3). The dysregulation of LDH-B and MCT-1 in both embryo and tissues of adults conceived by IVF strongly suggest an epigenetic regulation. Indeed, embryo

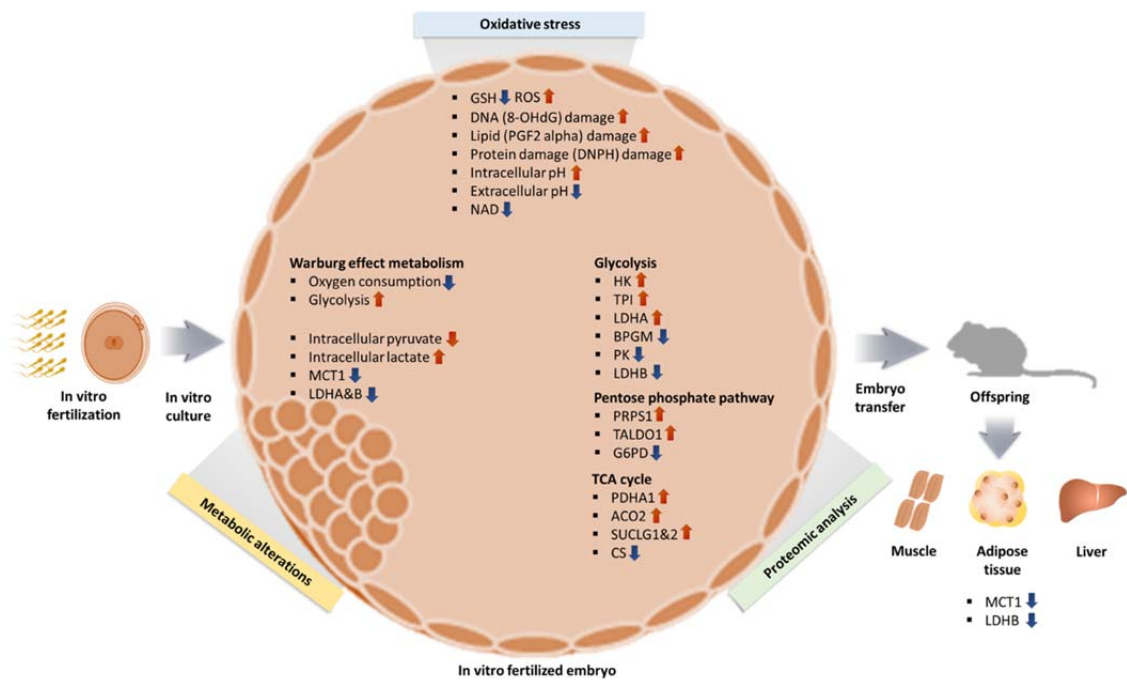
315 culture is associated with profound epigenetic changes (Doherty 2000; Reik, 2007; Reik 2001;
316 Ruggeri 2020).

317 In this work we have focused on studying the blastocyst stage, since this is the stage at which
318 human embryos are most commonly transferred. Future studies should examine how metabolic
319 differences, ROS and oxidative damage occur during earlier stages of embryo development, both
320 in mice and possibly human embryos. Although ROS production was documented after culture
321 of embryos using commercially available media even under conditions of low oxygen
322 concentration (Martin-Romero 2008), design of optimized culture media, aimed at reduce ROS
323 generation should be encouraged. In addition, a possible limitation of the paper has been the
324 prevalent utilization of fluorescence-based microscopy as a method to identify differences in
325 expression of oxidative marks or protein levels.

326 In summary, we can formulate a hypothesis in which (Figure 8) oxidative stress from in vitro
327 condition increase ROS and induce oxidative damage resulting in a shift toward Warburg
328 metabolism, given that lactate is a critical energy source (Brooks, 2018). The higher intracellular
329 lactate levels will likely induce epigenetic changes, to favor Warburg metabolism during
330 development, as an embryonic attempt to optimize growth based on the environment predicted to
331 be experienced in the future. A recent study (Yang 2021) showed that hypoxic embryo culture alters
332 histone lactylation marks (H3K23la, H3K18la), providing partial support to this hypothesis.

333 When the environment does not match the prediction, disease risk increases (Godfrey 2007).
334 Low lactate would be beneficial in a setting of low food resources because it could favor
335 lipolysis (Brooks, 2020). In fact, lactate activates the hydroxycarboxylic acid receptor 1
336 (HCAR1), a G protein-coupled receptor, which in turn inhibits lipolysis in fat cells via cAMP

and CREB (Liu 2009). However, since there is an abundance of food in our society, this mismatch could predispose IVF concepti to develop chronic disease like glucose intolerance.



343 4. Materials and Methods

344 Key resources table

Reagent type (species) or resource	Designation	Source or reference	Identifiers	Additional information
Antibody	Anti-8-Hydroxy-2-deoxyguanosine (Mouse monoclonal)	Abcam	Cat#: ab48508	IF (1:200)
Antibody	Anti-8 iso Prostaglandin F2 alpha (Rabbit polyclonal)	Abcam	Cat#: ab2280	IF (1:200)
Antibody	Anti-DNP antibody (Rabbit polyclonal)	Sigma	Cat#: D9656	IF (1:200)
Antibody	Anti-MCT1 antibody (Mouse monoclonal)	Santa Cruz	Cat#: sc365501	IF (1:200)
Antibody	Anti-LDHA antibody (Rabbit monoclonal)	Cell Signaling	Cat#: 3582	IF (1:200)
Antibody	Anti-LDHB antibody (Mouse monoclonal)	Santa Cruz	Cat#: sc100775	IF (1:200)
Antibody	Goat anti-Rabbit (goat polyclonal, Alexa Fluor conjugate)	Abcam	Cat#: ab150077	IF (1:200)
Antibody	Donkey anti-Rabbit (donkey polyclonal, Alexa Fluor conjugate)	Abcam	Cat#: ab150075	IF (1:200)
Antibody	Goat anti-Mouse (goat polyclonal, Alexa Fluor conjugate)	Abcam	Cat#: ab150113	IF (1:200)
Biological sample (mouse)	Blastocyst	This paper		Female
Biological sample (mouse)	Liver	This paper		Male/Female
Biological sample (mouse)	Muscle	This paper		Male/Female
Biological sample (mouse)	Fat	This paper		Male/Female
Commercial assay	Seahorse XF Cell	Agilent	103010-100	

or kit	Mito Stress Test kit			
Commercial assay or kit	Seahorse XF Glycolysis Stress Test kit	Agilent	103020-100	
Commercial assay or kit	Pyruvate assay kit	Cayman	Cat#: 700470	
Commercial assay or kit	Lactate assay kit	Cayman	Cat#: 700510	
Commercial assay or kit	NAD Quantitation kit	Sigma	Cat#: MAK037	
Chemical compound, drug	SNARF-1	Thermo fisher	Cat#: C1272	
Software, algorithm	GraphPad Prism	GraphPad		
Strain, strain background (mouse)	CF-1	ENVIGO	Hsd:NSA	Oocyte donor
Strain, strain background (mouse)	B6D2F1	The Jackson Laboratory	100006	Sperm donor

4.1. Embryo collection, *in vitro* fertilization and embryo culture

Animal experiments were approved by the Institutional Animal Care and Use Committee of the University of California, San Francisco, and all animals were maintained according to the institutional regulation under a 12 hour light/dark cycle with ad libitum access to water and food. In the present study, *in vitro* fertilization was performed as previously described (Feuer 2014b). In brief, 5 IU pregnant mare serum gonadotrophin (PMSG) was injected to CF1 female mice (8-9 weeks), and after 48 hours later, 5 IU human chorionic gonadotropin (hCG) was injected to those female mice for superovulation. Sperm were collected from the cauda epididymis in B6D2F1 male mice (8-9 weeks) and cumulus-oocyte complexes (COCs) were obtained from ampullae 13-14 hours after hCG administration. The COCs were incubated for 4 hours in human tubal fluid (HTF) medium (Millipore Corp; MR-070-D) with appropriate concentration of sperm obtained

following 1 hour capacitation. The fertilized embryos were washed in several drops of potassium simplex optimization medium (KSOM; Millipore, MR-106-D) and cultured in the same medium to the blastocyst stage at 37 °C under Ovoil™ (Vitrolife, #10029). In the present study, zygotes were cultured with different concentration of oxygen until blastocyst stage; 1) 37 °C, 5% CO₂ in humidified air, 5% oxygen (IVF 5% group), and 2) 37 °C, 5% CO₂ in humidified air, 20% oxygen (IVF 20% group). Control embryos (FB) were obtained from flushed blastocysts. Briefly, CF1 female mice (8–9 weeks) were superovulated with administration of 5 IU PMSG and 48 h later 5 IU hCG. Then, those females were mated to B6D2F1 males. The vaginal plug was checked after 14-18 hours and this was considered as Day 0.5. To control for the known delay in development after culture in vitro, for all experiments, only expanded blastocysts of similar morphology were used, as done before (Doherty 2000; Rinaudo 2006a; Rinaudo 2004). The in vivo-generated blastocysts were isolated by flushing 96-98 hours after hCG administration. IVF- 5% O₂ and 20% O₂ generated embryos reached the blastocyst stage after 96-98 hours following in vitro culture and 113-114 hours after hCG administration, respectively.

4.2. Evaluation of embryo development and a total cell number of blastocysts

The embryos were cultured for 4 days at 37 °C in a humidified atmosphere of different concentration of oxygen (5% and 20%). The evaluation of embryo development including cleavage rate and blastocyst formation rate from IVF and control groups were based on the morphology of the embryos and was approximately as follows, following hCG injection; 1) 2-cell: 16-18 h after IVF, and 2) blastocyst: 108-110 h. The blastocysts were stained with 5 µM of Hoechst 33342 for 7 min to count the total cell number in blastocysts. After washing in the phosphate buffer saline (PBS) medium, stained blastocysts were mounted on a glass slide in a

drop of glycerol with gentle compression using a cover slip. Cell counting was performed, and images were obtained under a Nikon scanning confocal microscope fitted with an ultraviolet lamp and 460nm/560nm excitation filter.

4.3. Redox status: Assessment of GSH/ROS levels in blastocyst

For quantification of intracellular ROS levels, blastocysts were washed twice in poly vinyl alcohol-phosphate buffered saline (PVA-PBS) (1 mg/ml) and incubated in 50 µl droplets of 10 µM 2',7'-dichlorodihydro-fluorescein diacetate (H2DCFDA, D6883, Sigma-Aldrich) in PVA-PBS for 15 min at 37 °C in an atmosphere of 5% CO₂. Then, the blastocysts were washed three times in PVA-PBS, and transferred to 10 µL droplets of PVA-PBS on a glass slide. Fluorescence intensity for ROS was measured under a Nikon scanning confocal microscope with a filter at 480 nm excitation and 510 nm emission. Evaluation of GSH levels followed same procedure, but the blastocysts were incubated in 10 µM 4-chloromethyl- 6,8- difluoro-7-hydroxycoumarin (CMF2HC; Cell Tracker Blue, Life Technologies, Carlsbad, USA). Fluorescence intensity for GSH was measured under a Nikon scanning confocal microscope with a filter at 371 nm excitation and 464 nm emission. The recorded fluorescence intensities were quantified using Image J software (version 1.48; National Institutes of Health, Bethesda, MD, USA) after deducting the background value. Total of 11-17 blastocysts were used in each group for five replications.

4.4. Assessment of ROS concentration in culture medium

ROS concentration in culture was assessed using an Oxiselect™ In vitro ROS/RNS Assay kit (Cell Biolabs, San Diego, CA, USA). The experiment was processed following the

manufacturer's instructions. Briefly, for measuring the total free radical presence in culture medium, the supernatant medium obtained from each group after IVC was obtained. Supernatant were transferred to 1.5 ml tubes and centrifuged at 10,000 g for 5 min to remove insoluble particles. The 50 µl of each supernatant was added to wells of a 96-well plate suitable for fluorescence measurement. Then 50 µl of catalyst was added to each well and incubated for 5 min at room temperature. Lastly, 100 µl of DCFH solution was added to each well followed by incubation at room temperature for 15 min and reading the fluorescence with a fluorescence plate reader at 480 nm excitation/530 nm emission (Soft Max Pro 4.7.1, Spectra max M2). The ROS concentrations were determined by comparison with the predetermined dichlorodihydrofluorescein (DCF) standard curve.

4.5. Assessment of Oxidative Stress by Immunofluorescence

Immunofluorescence staining was performed to evaluate the degree of oxidative stress in blastocysts derived from each group. Blastocysts were washed three times in PBS containing 0.2% PVA and fixed with 4% paraformaldehyde (w/v) in PBS for 30 min at room temperature. All steps were performed at room temperature unless otherwise stated. After washing three times in PBS, blastocysts were permeated with 1% (v/v) Triton X-100 in PBS for 2 hr. Then, the samples were washed three times in PBS and blocked with 2% BSA in PBS for 4 hr. at 4°C. The blastocysts were incubated with primary antibodies for 8-Hydroxy-2-deoxyguanosine (8-OHdG, 1:200; ab48508, Abcam), 8-iso Prostaglandin F2 alpha (PGF2 alpha, 1:200; ab2280, Abcam), and 2,4-Dinitrophenylhydrazine (DNPH, 1:200; D9656, Sigma), monocarboxylic acid transporter 1 (MCT1, 1:200; sc-365501, Santa Cruz), lactate dehydrogenase A (LDHA, 1:200; #3582, Cell Signaling), lactate dehydrogenase B (LDHB, 1:200; sc-100775, Santa Cruz) at 4°C

overnight. Blastocysts were then washed three times in PBS with 2% BSA and then incubated with a secondary anti-rabbit antibody (1:200, ab150077, Abcam; 1:200, ab150075, Abcam) or anti-mouse antibody (1:200; ab150113, Abcam) for 3 hr. at room temperature. After washing three times in PBS with 2% BSA, the samples were mounted on glass slides. Images were captured under a Nikon scanning confocal microscope with the same exposure times and adjustments. The intensities of 8-OHdG, PGF2 alpha, DNPH, MCT1, LDHA, LDHB were measured by Image J software (version 1.46r; National Institutes of Health). For the intensities of 8-OHdG, PGF2 alpha, DNPH, total of 26-27 blastocysts were used in each group for at least three replications. For the intensities of MCT1, LDHA, LDHB, total of 31-33 blastocysts were used in each group for at least three replications.

4.6. Metabolic profile analyses in blastocysts

Metabolic function in blastocysts were carried out using Agilent Seahorse XF HS Mini Analyzer (Agilent, Santa Clara, CA, USA) according to the manufacturer's instruction. Briefly, for plate hydration, 200 µl of distilled water was added to the sensor-containing Seahorse 8-well fluxpaks (Agilent Technology), which were coated with Poly-D-Lysine, were incubated overnight at 37 °C in a non-CO₂ humidified incubator. Ten blastocysts were incubated in XF base assay media supplemented with 1 mM glutamine, 0.2 mM glucose, 0.2 mM pyruvate, and incubated at 37 °C in a non-CO₂ humidified incubator for 1 h to allow to pre-equilibrate with the assay medium. For real-time ATP rate analysis, 1.5 µM oligomycin (ATP synthase inhibitor) and 0.5 µM rotenone/antimycin A (Complex I/III inhibitor) were sequentially injected after incubation. For mitochondrial respiration analysis, 1.5 µM oligomycin, 1 µM Carbonyl cyanide-4-trifluoromethoxyphenylhydrazone (FCCP, a potent uncoupler of oxidative phosphorylation), and

0.5 μ M rotenone/antimycin A were sequentially injected. Meanwhile, 0.5 μ M rotenone/antimycin A and 50 mM 2-deoxy-D-glucose (2-DG, glycolysis inhibitor) were injected for glycolytic rate analysis. Oligomycin inhibits ATP-synthase and can be considered as indicator of the proportion of O_2 consumption directly coupled to ATP generation. FCCP is a potent mitochondrial uncoupler which dissipates the proton gradient between the intermembrane and the matrix in mitochondria allowing the maximal oxygen consumption rate (OCR) measurement. As complex I/III inhibitors, rotenone and antimycin A combine to inhibit the electron transport chain entirely, therefore, the proportion of OCR after the addition of rotenone/antimycin A is considered to be non-mitochondrial effect. 2-DG is a glucose analog which inhibits glycolysis through competitive binding of glucose hexokinase in the glycolytic pathway. These measurements were used to determine the magnitudes of various parameters of OCR, ECAR, ATP rate, mitochondrial respiration rate, and glycolytic rate based on the targets of each successive drug injection. Extracellular acidification rate (ECAR) is the sum of two components: respiratory acidification, in the form of CO_2 (which hydrates to H_2CO_3 then dissociates to $HCO_3^- + H^+$), and glycolytic acidification, in the form of lactate- + H^+ .

4.7. Measurement of intracellular/extracellular pH in blastocyst and culture medium

Intracellular pH was determined by using the pH-sensitive fluorophore, SNARF-1 (esterified derivative; Molecular Probes, Eugene, OR), loaded into blastocysts by incubating them with 5 μ M SNARF-1 at 37°C for 20 min in KSOM (Edwards 1998a) . After SNARF-1 staining, blastocysts (7-13 blastocysts per group, in triplicates) were washed with fresh KSOM and placed in a temperature-controlled chamber. Two fluorescence emission wavelengths were detected, 640 nm (pH sensitive) and 600 nm (pH insensitive), using an excitation wavelength of 535 nm.

The ratio of the two emission intensities was calculated by dividing the images after background subtraction. At the conclusion of each experiment, the ratio was converted to an actual intracellular pH value using the calibration standard curve, where intracellular pH is clamped to known extracellular values using the ionophores, nigericin (10 μ g/ml). The SNARF-1 staining and exposure to excitation illumination does not adversely affect the blastocyst, as previous research demonstrated that mouse embryos normally cleaved following pH measurements (Edwards 1998a). To control for the possible variation in blastocoel size in different embryos, we compared immunofluorescence level of only the inner cell mass and trophoblast region of blastocysts and excluded the blastocoel region.

The extracellular pH level of the culture medium was measured in 30 μ l of fluid in which 20 embryos were cultured for 4.5 days by using a pH electrode with a small tip (3 mm in diameter, Orion Ross Electrode, Thermo Scientific, USA) attached to an Accumet basic AB15 pH meter (Mettler Toledo, USA). Briefly, two buffer calibrations (pH 7 and 10) were performed at same temperature as the sample. After calibration, rinse the electrode with distilled water and then place the electrode into the 30 μ l of sample. When the reading is stable, pH level was recorded.

4.8. Assessment of nicotinamide adenine dinucleotide (NAD) concentration in blastocysts

Nicotinamide adenine dinucleotide (NAD) concentration was measured using the NAD Quantitation kit (MAK037, Sigma-Aldrich, MO, USA). In brief, NADH (Reduced form of NAD)/NAD was extracted from blastocysts by using NADH/NAD extraction buffer with freeze/thawing for 2 cycles of 20 minutes on dry ice. The mixture was centrifuged at 13,000 x g for 10 min to remove insoluble material. The NAD/NADH supernatant was transferred into a 1.5 ml Eppendorf tube. The 50 μ l of extracted samples were transferred into a 96 well plate. Then,

100 µl of the master reaction mix were added to each well and incubated for 5 min at room temperature to convert NAD to NADH for NAD_{total} determinations. Finally, 10 µl of NADH developer were added into each well and incubated at room temperature for 1-4 hrs. The reactions were stopped by adding 10 µl of stop solution into each well and mixing well. The measurement was performed at 450 nm by using microplate reader (Soft Max Pro 4.7.1, Spectra max M2).

4.9. Assessment of pyruvate and lactate level in blastocyst and culture media

As another measure of cytosolix redox state, intracellular and extracellular pyruvate and lactate level were measured in blastocysts and culture medium respectively following manufacturer's instructions (Pyruvate assay kit, Cayman Chemical, MI, USA; Lactate assay kit, Cayman Chemical, MI, USA). To collect 300 blastocysts, we performed multiple IVF, each IVF resulting in 10-20 blastocysts cultured in 30 microliters of media. While intracellular lactate and pyruvate were performed on the embryos collected, the media from different experiments was pooled to a final 500 microliter volume. For sample preparation, the 500 µl of embryo culture medium was collected for measurement of extracellular pyruvate/lactate level. To deproteinate the sample, 500 µl of 0.5 M metaphosphoric acid (MPA) were added and the specimen was placed on ice for 5 min. Then, the mixture was centrifuged at 10,000 x g for 5 min at 4 °C to pellet the proteins. The supernatant was removed and the 50 µl of potassium carbonate was added to neutralize the acid. The sample was centrifuged at 10,000 x g for 5 min at 4 °C and the supernatant removed for assaying.

For measurement of intracellular pyruvate/lactate levels in blastocysts, 0.5 ml of 0.25 M MPA were added to blastocysts and placed on ice for 5 min. Three- hundred blastocysts per group

were used to perform this experiment (900 total). Then, the sample was centrifuged at 10,000 x g for 5 min at 4 °C and the supernatant was removed for assaying. Then, 50 µl of assay buffer, 50 µl of cofactor mixture, 10 µl of fluorometric detector, and 20 µl of samples were added to each well. The reactions were initiated by adding 20 µl of enzyme mixture to all of the wells being used. Thereafter, the plate was incubated for 20 min at room temperature and then read using an excitation wavelength between 530-540 nm and emission wavelength between 585-595 nm by using microplate reader (Soft Max Pro 4.7.1, Spectra max M2). For the lactate assay, 20 µl of sample was added to each well. Then, 100 µl of diluted assay buffer, 20 µl of cofactor mixture, and 20 µl of fluorometric substrate were added to all wells being used. The 40 µl of enzyme mixture was added to initiate the reactions. Lastly, the plate was incubated for 20 min at room temperature and the fluorescence was read using an excitation wavelength between 530-540 nm and emission wavelength between 585-595 nm with microplate reader (Soft Max Pro 4.7.1, Spectra max M2).

4.10. Proteomic analyses

Experiments were conducted in triplicates (n=100 blastocyst for each replicate). Proteins were extracted with 8M urea, 50 mM ammonium bicarbonate and Benzonase 24U/100ml), reduced with TCEP, alkylated with iodoacetamide, and digested overnight with Trypsin/Lys-C mix followed by desalting with C18 cartridges in an automated fashion using an AssayMap BRAVO (Agilent). Peptide mixture was analyzed by LC-MS/MS using a Proxeon EASY nanoLC system (Thermo Fisher Scientific) coupled to an Orbitrap Fusion Lumos mass spectrometer equipped with FAIMS Pro device (Thermo Fisher Scientific). Peptides were separated using an analytical C18 Aurora column (75µm x 250 mm, 1.6µm particles; IonOpticks) at a flow rate of 300 nL/min

using a 140-min gradient: 1% to 6% B in 1 min, 6% to 23% B in 90 min, 23% to 34% B in 48 min, and 34% to 50% B in 1 min (A= FA 0.1%; B=80% ACN: 0.1% FA). The mass spectrometer was operated in positive data-dependent acquisition mode, and the Thermo FAIMS Pro device was set to standard resolution. A three-experiment method was set up where each experiment utilized a different FAIMS Pro compensation voltage: - 50, -70, and -80 Volts, and each of the three experiments had a 1 second cycle time. A high-resolution MS1 scan in the Orbitrap (m/z range 350 to 1,500, 120k resolution at m/z 200, AGC 4e5 with maximum injection time of 50 ms, RF lens 30%) was collected in top speed mode with 1-second cycles for the survey and the MS/MS scans. For MS2 spectra, ions with charge state between +2 and +7 were isolated with the quadrupole mass filter using a 0.7 m/z isolation window, fragmented with higher-energy collisional dissociation with normalized collision energy of 30%, and the resulting fragments were detected in the ion trap as rapid scan mode with AGC of 5e4 and maximum injection time of 35 ms. The dynamic exclusion was set to 20 sec with a 10 ppm mass tolerance around the precursor.

Mass spectra were analyzed with SpectroMine software (Biognosys, version 2.7.210226.47784). Search criteria used were: full tryptic specificity (cleavage after lysine or arginine residues unless followed by proline), missed cleavages were allowed, carbamidomethylation (C) was set as fixed modification and oxidation (M) as a variable modification. The false identification rate was set to 1%. Quality control, Relative quantification, and downstream analysis were performed using the artMS Bioconductor package, which uses MSstats for normalization and differential analysis (Choi 2014). Pathway enrichment analysis was performed using the PathView Bioconductor package (Luo 2013).

4.11. Western Blotting

Extracts for SDS-PAGE were prepared from whole gonadal fat, muscle (gastrocnemius) or liver tissues of 40 weeks old mice generated in vivo (FB, n=8, 50% females) or by IVF (n=8, 50% females) after culture in 5% oxygen (Feuer 2014b). In addition, each individual tissue sample had the blot repeated 4 times (= 4 technical replicates): the average of the 4 measurements was used as the mean intensity for that sample.

Of note, we did not generate a cohort of adult mice by IVF after culture in 20% oxygen. Tissues were homogenized in cold tissue extraction buffer (100mM Tris, 2mM Na₃VO₄, 100mM NaCl, 1% Triton X-100, 1mM EDTA, 10% glycerol, 1% EGTA, 0.1% SDS, 1mM NaF, 0.5% deoxycholate, 20% Na₄P₂O₇, with protease inhibitors). Protein levels were quantified by BCA protein assay (Thermo Scientific). 15µg tissue were subjected to gel electrophoresis on 12% PAGEr™ Gold Precast gels (Lonza) and blotted on to Immobilon-FL membranes (Millipore) using semi-dry transfer (Bio-Rad). Dried membranes were reactivated in methanol, rinsed with PBS, and blocked in Odyssey Blocking Buffer (LI-COR Biosciences, 927-40000). Membranes were then probed overnight at 4°C with primary antibodies diluted 1:1000 in blocking buffer with 0.1% Tween-20, washed in PBS and incubated with secondary antibody diluted in blocking buffer containing 0.1% SDS and 0.1% Tween20. Protein signal detection was performed using the LI-COR Odyssey Imaging System.

4.12. Statistical analyses

Experiments were performed in triplicates. Only lactate and pyruvate levels were measured in a single biological replicate with 10 technical replicates, given the large number of embryos needed. All data were analyzed by the One-way analysis of variance with Tukey's multiple

588 comparison test or unpaired t-test using GraphPad Prism 9.0 (GraphPad, San Diego, CA) were
589 applied to analyze the experimental data. All data are expressed as the means values \pm standard
590 deviation. Differences were considered statistically significant if $p < 0.05$.

591 **Acknowledgments**

592 The authors wish to thank Dr. Diane Barber and Dr. Yi for their help in optimizing intracellular
593 pH measurements and Dr George Brooks for the helpful feedback on the manuscript.

594

595 **Author contributions**

596 PFR designed the study. SHL and PFR conceived the experiments. SHL, XL, and DJM
597 conducted the experiments. All authors analyzed the data and results. All authors wrote and
598 reviewed the manuscript.

599

600 **Competing interests**

601 The authors declare that there is no conflict of interest that could be perceived as prejudicing the
602 impartiality of the research reported.

603

604 **Data availability**

605 All data generated or analyzed during this study are included in the manuscript and supporting
606 file.

607

608 **Funding**

609 This work was funded by R01 R01HD092267 to PFR

610

611 **Correspondence**

612 Please send correspondence to Paolo F. Rinaudo.

Figure Legends

Figure 1. (A) Analysis of GSH and ROS in blastocysts. (B) GSH levels are lower in IVF-generated blastocysts, while ROS levels are higher both (C) intracellularly and (D) extracellularly. Since FB were not cultured, the ROS value for the FB group is missing. Data are shown as means \pm S.D and at least three independent replicates were performed. One asterisk (*) if $p < 0.05$. Three and four asterisks (***) and *****) if $p < 0.001$ and <0.0001 , respectively. Bar = 50 μ m.

Figure 2. Immunocytochemical analysis of oxidative-related markers in blastocysts. (A and B) IVF generated blastocysts show increase in 8-OHdG staining (DNA damage marker, green), (C and D) PGF2-alpha (lipid damage marker, green) and (E and F) DNPH staining (protein damage marker, green) compared to in vivo control embryos.

Data are shown as means \pm S.D and at least three independent replicates were performed. * if $p < 0.05$; ** if $p < 0.01$, *** if $p < 0.001$ and *****) if $p < 0.0001$. Bar = 50 μ m.

Figure 3. Metabolic analysis of mitochondrial and glycolytic function using Agilent Seahorse XF HS Mini. (A) Mitochondrial respiration was analyzed at baseline, or after injection of oligomycin (ATP synthase inhibitor), carbonyl cyanide-p-trifluoromethoxyphenylhydrazone (FCCP, an uncoupler of oxidative phosphorylation), and rotenone/antimycin A (Complex I/III inhibitors). (B) IVF-generated blastocysts show reduced basal oxygen consumption rate (FB: 2.3 ± 0.2 pmol/min/blastocyst, IVF5%O₂: 2.0 ± 0.2 pmol/min/blastocyst, IVF20%O₂: 1.5 ± 0.2 pmol/min/blastocyst), (C) ATP production (FB: 1.6 ± 0.1 pmol/min/blastocyst, IVF5%O₂: 1.2 ± 0.1 pmol/min/blastocyst, IVF20%O₂: 0.9 ± 0.3 pmol/min/blastocyst) and (D) maximal

respiration (FB: 4.0 ± 0.2 pmol/min/blastocyst, IVF5%O₂: 2.9 ± 0.2 pmol/min/blastocyst, IVF20%O₂: 2.5 ± 0.2 pmol/min/blastocyst) compared to in vivo- generated embryos. **(E)** Glycolysis was studied at baseline or after injection of rotenone/antimycin and 2-deoxy-D-glucose (2-DG, glycolysis inhibitor). **(F)** IVF generated embryos showed increase in basal glycolysis (FB: 1.3 ± 0.0 pmol/min/blastocyst, IVF5%O₂: 1.5 ± 0.1 pmol/min/blastocyst, IVF20%O₂: 1.7 ± 0.1 pmol/min/blastocyst), **(G)** basal proton efflux rate (FB: 2.7 ± 0.0 pmol/min/blastocyst, IVF5%O₂: 3.2 ± 0.2 pmol/min/blastocyst, IVF20%O₂: 3.7 ± 0.0 pmol/min/blastocyst) and **(H)** compensatory glycolysis rate (FB: 0.8 ± 0.0 pmol/min/blastocyst, IVF5%O₂: 0.9 ± 0.1 pmol/min/blastocyst, IVF20%O₂: 1.1 ± 0.1 pmol/min/blastocyst) compared to in vivo generated embryos. Overall, IVF embryos utilize more glycolysis and less oxidative phosphorylation to generate energy. **(I)** Bar chart of blastocysts ranked by OCR to ECAR ratio along the x axis. **(J)** Energy maps of blastocysts. Data are shown as means \pm S.D and at least three independent replicates were performed. Different superscript indicates statistically significant differences. * if $p < 0.05$; ** if $p < 0.01$, *** if $p < 0.001$ and **** if $p < 0.0001$.

Figure 4. IVF-generated embryos show several metabolic alterations. **(A)** Confocal microscopy images of blastocysts using phase contrast or confocal microscopy. Two fluorescence emission wavelengths were used, 640 nm (pH sensitive, green) and 600 nm (pH insensitive, yellow) with an excitation wavelength of 535 nm. **(B)** IVF-generated embryos show higher intracellular pH and **(C)** lower extracellular pH in culture medium. Of note extracellular pH levels of in vivo-generated embryos are missing since in vivo embryos are not cultured. **(D)** IVF-generated embryos also showed reduction in NAD levels and **(E)** intracellular pyruvate levels, but higher intracellular lactate **(F)**. Values are mean \pm standard deviation. Data are shown as the means \pm

S.D and at least three independent replicates were performed except pyruvate and lactate assay. For pyruvate and lactate assay, total 300 blastocysts were used for one biological replication and seven technical replications. * if $p < 0.05$; ** if $p < 0.01$, *** if $p < 0.001$ and **** if $p < 0.0001$. Bar = 50 μm .

Figure 5. Analysis of glycolysis, pentose phosphate pathway (PPP) and tricarboxylic acid (TCA) cycle proteins dysregulated in IVF-generated blastocysts vs control. Overall, 3,965 proteins were identified and 1,029 were differentially expressed between the groups. IVF5%O₂- generated blastocysts had 334 proteins upregulated relative to the control (FB), while 499 proteins were upregulated on IVF20%O₂ embryos, with 85% overlap.

Six glycolytic proteins had different levels in IVF embryos compared to control. Hexokinase 2 (HK) and triosephosphate isomerase 1 (TPI) were upregulated, while 2,3-bisphosphoglycerate mutase (BPGM), pyruvate kinase (PK), and LDHB were downregulated in both IVF groups compared to in vivo generated blastocysts. In addition, LDHA isoenzyme was upregulated only in IVF5%O₂ blastocysts compared to control.

Three proteins involved in the pentose phosphate pathway were different between IVF embryos and control embryos. Glucose 6-phosphate dehydrogenase (G6PD) was decreased in both IVF groups, while phosphoribosyl pyrophosphate synthetase 1 (PRPS1) and transaldolase 1 (TALDO1) were higher in IVF5%O₂ – generated blastocysts compared to control.

Four proteins associated with TCA cycle were significantly dysregulated in IVF-generated embryos. Succinyl-CoA ligase α (SUCLG1) was significantly upregulated in both IVF group compared to in vivo embryos. The remaining proteins were dysregulated only in IVF20%O₂- generated embryos compared to control: pyruvate dehydrogenase (PDHA1), aconitase (ACO2),

and succinyl-CoA ligase β (SUCLG2) were upregulated, while citrate synthase (CS) was downregulated.

Proteins are highlighted in blue color if they were statistically different ($p < 0.05$) in both IVF groups compared to control; yellow color indicates changes of only IVF5%O₂ - generated blastocysts vs in vivo embryo; red color indicates changes of only IVF20%O₂ - generated blastocysts vs in vivo embryo; black arrows represent the directionality of the interaction (increased or decreased).

Figure 6. IVF-generated embryos show downregulation of enzymes involved in lactate metabolism. **(A)** Expression levels of LDHA and LDH-B (red color: LDHA, green color: LDHB) and **(B and C)** their quantification. **(D and E)** MCT1 enzyme is downregulated in IVF embryos compared to control. The expression level of LDHB and MCT1 was decreased in IVF20%O₂ compared to IVF5%O₂ blastocysts. Data are presented as means \pm S.D and at least three independent replicates were performed. * if $p < 0.05$; ** if $p < 0.01$, *** if $p < 0.001$ and **** if $p < 0.0001$. Bar = 50 μ m.

Figure 7. Western blot analysis of protein levels of LDH-B and MCT1 enzymes in selected insulin sensitive tissues of 40-week-old mice conceived in vivo (FB n=8, 50% females) or by IVF5%O₂ (n=8, 50% females). IVF-conceived mice show reduced levels of LDHB and MCT 1 in gastrocnemius muscle **(A-C)** gonadal adipose tissue **(D-F)** and liver **(G-I)**. Selected blots are shown. Data are presented as means \pm S.D and at least three independent replicates were performed. * if $p < 0.05$; ** if $p < 0.01$.

Figure 8. Summary of changes observed in IVF generated blastocysts and offspring. IVF generated embryos show increase in ROS and oxidative damage and significant metabolic derangement including decreased NAD levels, increased intracellular pH and contemporaneous decrease in extracellular pH and increased Warburg metabolism. Ultimately, IVF-generated embryos show increased intracellular lactate levels, likely secondary to decreased level of MCT1, LDH-A and LDH-B enzymes. Of note, adult mice conceived by IVF also show decreased levels of MCT1 and LDH-B.

Supplemental Figure 1. Morphology of blastocyst generated after natural mating (in vivo or flushed blastocyst-FB-group, **A**) or by IVF using physiologic oxygen (**B**: IVF 5%O₂ group), or IVF 20%O₂ (**C**: IVF 20%O₂ group). In addition, (**D**) embryos generated by IVF and cultured in physiologic oxygen (5% O₂), showed higher 2-cell rate ($71.0 \pm 3.1\%$, $p < 0.0001$) and (**E**) blastocyst rate ($82.8 \pm 10.9\%$, $p < 0.0001$) compared to embryos cultured under 20% O₂ ($51.8 \pm 9.3\%$, $p < 0.0001$ and $57.5 \pm 11.6\%$, $p < 0.0001$, respectively). (**F**) IVF generated blastocysts had lower total cell number (IVF 5%O₂: 58.1 ± 10.8 ; IVF 20% O₂ 47.5 ± 10.9), compared to in vivo generated blastocysts (70.6 ± 11.3 , $p < 0.05$). Data are shown as means \pm S.D. A total of 11 independent replicates were performed. One asterisk (*) indicates p value smaller than 0.05. Three and four asterisks (***) indicate p value smaller than 0.001 and 0.0001, respectively.

Supplemental Figure 2. Lactate (**A**) and pyruvate (**B**) levels are lower in media where IVF-generated embryos are cultured compared to media maintained in incubator without embryos. Seven biological replications were performed for each experiment. * if $p < 0.05$; ** if $p < 0.01$, *** if $p < 0.001$ and **** if $p < 0.0001$.

Supplemental Figure 3. Unsupervised metabolomic analysis by LC/MS was performed in liver, gonadal adipose tissue and serum of in vivo conceived mice or mice conceived by IVF (5%O₂) Data are from (Feuer 2014b) and at least three independent replicates were performed. Relative lactic acid levels trend lower in IVF conceived mice.

Source data

Figure 1-source data 1. The ROS and GSH level in embryos (Figure 1A-C).

Figure 1-source data 2. The extracellular ROS level in embryo culture medium (Figure 1D).

Figure 2-source data 1. The level of oxidative damage (DNA, lipids, and proteins) in embryos (Figure 2A-F).

Figure 3-source data 1. The mitochondrial activity in embryos (Figure 3A).

Figure 3-source data 2. The mitochondrial activity in embryos (Figure 3B-D).

Figure 3-source data 3. The glycolytic function in embryos (Figure 3E-H).

Figure 3-source data 4. The ratio of oxygen consumption rate and extracellular acidification rate in embryos (Figure 3I-J).

Figure 4-source data 1 Intracellular pH level in embryos (Figure 4A-B).

746 Figure 4-source data 2. The NAD level in embryos (Figure 4D).

747 Figure 4-source data 3. The intracellular pyruvate level in embryos (Figure 4E).

748 Figure 4-source data 4. The intracellular lactate level in embryos (Figure 4F).

749 Figure 5-source data 1. The proteomic analysis data (Figure 5).

750 Figure 6-source data 1. The fluorescence intensity of LDHB, LDHA, and MCT1 in embryos

751 (Figure 6A-E).

752 Figure 7- source data. Eight biological replicates for FB and IVF were compared. The value of

753 each biological replicate was the average of 4 technical replicates.

- 754 - Muscle
 - 755 ○ Western blot images (ppt)
 - 756 ○ source data (xls)
- 757 - Fat
 - 758 ○ Western blot images (ppt)
 - 759 ○ source data (xls)
- 760 - Liver
 - 761 ○ Western blot images (ppt)
 - 762 ○ source data (xls)

763 Supplemental Figure 1-source data 1. The cleavage and blastocyst rate in embryos (Figure 1D-

764 E).

765 Supplemental Figure 1-source data 2. The total cell number of blastocysts (Figure 1F).

766 Supplemental Figure 2-source data 1. The extracellular lactate and pyruvate level in embryo
767 culture medium (Supplemental Figure 2A-B).

768 Supplemental Figure 3-source data 1. The lactate level in liver, fat, and serum in adult mice.

769 References

- 770 **Acton, BM, A Jurisicova, I Jurisica, and RF Casper** 2004 Alterations in mitochondrial membrane potential
 771 during preimplantation stages of mouse and human embryo development. *Mol Hum Reprod* **10**
 772 23-32.
- 773 **Adam, AA, Y Takahashi, S Katagiri, and M Nagano** 2004 In vitro culture of mouse preantral follicles
 774 using membrane inserts and developmental competence of in vitro ovulated oocytes. *J Reprod*
 775 *Dev* **50** 579-586.
- 776 **Auerbach, S, and RL Brinster** 1967 Lactate dehydrogenase isozymes in the early mouse embryo. *Exp Cell*
 777 *Res* **46** 89-92.
- 778 **Bavister, B** 2004 Oxygen concentration and preimplantation development. *Reprod Biomed Online* **9** 484-
 779 486.
- 780 **Becker, HM, and JW Deitmer** 2021 Proton Transport in Cancer Cells: The Role of Carbonic Anhydrases.
 781 *Int J Mol Sci* **22**.
- 782 **Belli, M, L Zhang, X Liu, A Donjacour, E Ruggeri, MG Palmerini, SA Nottola, G Macchiarelli, and P**
 783 **Rinaudo** 2019 Oxygen concentration alters mitochondrial structure and function in in vitro
 784 fertilized preimplantation mouse embryos. *Hum Reprod* **34** 601-611.
- 785 **Berntsen, S, V Soderstrom-Anttila, UB Wennerholm, H Laivuori, A Loft, NB Oldereid, LB Romundstad, C**
 786 **Bergh, and A Pinborg** 2019 The health of children conceived by ART: 'the chicken or the egg?'.
 787 *Hum Reprod Update* **25** 137-158.
- 788 **Bertoldo, MJ, DR Listijono, WJ Ho, AH Riepsamen, DM Goss, D Richani, XL Jin, S Mahbub, JM Campbell,**
 789 **A Habibalahi, WN Loh, NA Youngson, J Maniam, ASA Wong, K Selesniemi, S Bustamante, C Li,**
 790 **Y Zhao, MB Marinova, LJ Kim, L Lau, RM Wu, AS Mikolaizak, T Araki, DG Le Couteur, N Turner,**
 791 **MJ Morris, KA Walters, E Goldys, C O'Neill, RB Gilchrist, DA Sinclair, HA Homer, and LE Wu**
 792 2020 NAD(+) Repletion Rescues Female Fertility during Reproductive Aging. *Cell Rep* **30** 1670-
 793 1681 e1677.
- 794 **Brooks, GA** 2018 The Science and Translation of Lactate Shuttle Theory. *Cell Metab* **27** 757-785.
- 795 **Brooks, GA** 2020 Lactate as a fulcrum of metabolism. *Redox Biol* 101454.
- 796 **Cebral, E, I Carrasco, D Vantman, and R Smith** 2007 Preimplantation embryotoxicity after mouse
 797 embryo exposition to reactive oxygen species. *Biocell* **31** 51-59.
- 798 **Ceelen, M, MM van Weissenbruch, J Prein, JJ Smit, JP Vermeiden, M Spreeuwenberg, FE van Leeuwen,**
 799 **and HA Delemarre-van de Waal** 2009 Growth during infancy and early childhood in relation to
 800 blood pressure and body fat measures at age 8-18 years of IVF children and spontaneously
 801 conceived controls born to subfertile parents. *Hum Reprod* **24** 2788-2795.
- 802 **Ceelen, M, MM van Weissenbruch, JP Vermeiden, FE van Leeuwen, and HA Delemarre-van de Waal**
 803 2008 Cardiometabolic differences in children born after in vitro fertilization: follow-up study. *J*
 804 *Clin Endocrinol Metab* **93** 1682-1688.
- 805 **Chatel, B, D Bendahan, C Hourde, L Pellerin, S Lengacher, P Magistretti, Y Le Fur, C Vilmen, M Bernard,**
 806 **and LA Messonnier** 2017 Role of MCT1 and CAII in skeletal muscle pH homeostasis, energetics,
 807 and function: in vivo insights from MCT1 haploinsufficient mice. *Faseb J* **31** 2562-2575.
- 808 **Choi, M, CY Chang, T Clough, D Broudy, T Killeen, B MacLean, and O Vitek** 2014 MSstats: an R package
 809 for statistical analysis of quantitative mass spectrometry-based proteomic experiments.
 810 *Bioinformatics* **30** 2524-2526.
- 811 **Christianson, MS, Y Zhao, G Shoham, I Granot, A Safran, A Khafagy, M Leong, and Z Shoham** 2014
 812 Embryo catheter loading and embryo culture techniques: results of a worldwide Web-based
 813 survey. *J Assist Reprod Genet* **31** 1029-1036.

- Chronopoulou, E, and JC Harper** 2015 IVF culture media: past, present and future. *Hum Reprod Update* **21** 39-55.
- Ciray, HN, T Aksoy, K Yaramanci, I Karayaka, and M Bahceci** 2009 In vitro culture under physiologic oxygen concentration improves blastocyst yield and quality: a prospective randomized survey on sibling oocytes. *Fertil Steril* **91** 1459-1461.
- Cui, L, M Zhao, Z Zhang, W Zhou, J Lv, J Hu, J Ma, M Fang, L Yang, CG Magnussen, B Xi, and ZJ Chen** 2021 Assessment of Cardiovascular Health of Children Ages 6 to 10 Years Conceived by Assisted Reproductive Technology. *JAMA Netw Open* **4** e2132602.
- Doherty, AS, MR Mann, KD Tremblay, MS Bartolomei, and RM Schultz** 2000 Differential effects of culture on imprinted H19 expression in the preimplantation mouse embryo. *Biol Reprod* **62** 1526-1535.
- Donjacour, A, X Liu, W Lin, R Simbulan, and PF Rinaudo** 2014 In vitro fertilization affects growth and glucose metabolism in a sex-specific manner in an outbred mouse model. *Biol Reprod* **90** 80.
- Edwards, LJ, DA Williams, and DK Gardner** 1998a Intracellular pH of the mouse preimplantation embryo: amino acids act as buffers of intracellular pH. *Hum Reprod* **13** 3441-3448.
- Edwards, LJ, DA Williams, and DK Gardner** 1998b Intracellular pH of the preimplantation mouse embryo: effects of extracellular pH and weak acids. *Mol Reprod Dev* **50** 434-442.
- Feuer, S, X Liu, A Donjacour, R Simbulan, E Maltepe, and P Rinaudo** 2016 Common and specific transcriptional signatures in mouse embryos and adult tissues induced by in vitro procedures. *Reproduction*.
- Feuer, SK, A Donjacour, RK Simbulan, W Lin, X Liu, E Maltepe, and PF Rinaudo** 2014a Sexually dimorphic effect of in vitro fertilization (IVF) on adult mouse fat and liver metabolomes. *Endocrinology* **155** 4554-4567.
- Feuer, SK, X Liu, A Donjacour, W Lin, RK Simbulan, G Giritharan, LD Piane, K Kolahi, K Ameri, E Maltepe, and PF Rinaudo** 2014b Use of a Mouse In Vitro Fertilization Model to Understand the Developmental Origins of Health and Disease Hypothesis. *Endocrinology* **155** 1956-1969.
- Frederick, DW, E Loro, L Liu, A Davila, Jr., K Chellappa, IM Silverman, WJ Quinn, 3rd, SJ Gosai, ED Tichy, JG Davis, F Mourkioti, BD Gregory, RW Dellinger, P Redpath, ME Migaud, E Nakamaru-Ogiso, JD Rabinowitz, TS Khurana, and JA Baur** 2016 Loss of NAD Homeostasis Leads to Progressive and Reversible Degeneration of Skeletal Muscle. *Cell Metab* **24** 269-282.
- Gardner, DK, and PL Wale** 2013 Analysis of metabolism to select viable human embryos for transfer. *Fertil Steril* **99** 1062-1072.
- Gardner, PR, and I Fridovich** 1991 Superoxide sensitivity of the Escherichia coli 6-phosphogluconate dehydratase. *J Biol Chem* **266** 1478-1483.
- Gatenby, RA, and RJ Gillies** 2008 A microenvironmental model of carcinogenesis. *Nat Rev Cancer* **8** 56-61.
- Gillies, RJ, D Verduzco, and RA Gatenby** 2012 Evolutionary dynamics of carcinogenesis and why targeted therapy does not work. *Nat Rev Cancer* **12** 487-493.
- Godfrey, KM, KA Lillycrop, GC Burdge, PD Gluckman, and MA Hanson** 2007 Epigenetic Mechanisms and the Mismatch Concept of the Developmental Origins of Health and Disease. *Pediatric Research* **61** 5R-10R.
- Goldsmith, S, S McIntyre, N Badawi, and M Hansen** 2018 Cerebral palsy after assisted reproductive technology: a cohort study. *Dev Med Child Neurol* **60** 73-80.
- Gongadashetti, K, P Gupta, R Dada, and N Malhotra** 2021 Follicular fluid oxidative stress biomarkers and ART outcomes in PCOS women undergoing in vitro fertilization: A cross-sectional study. *Int J Reprod Biomed* **19** 449-456.
- Goto, Y, Y Noda, T Mori, and M Nakano** 1993 Increased generation of reactive oxygen species in embryos cultured in vitro. *Free Radic Biol Med* **15** 69-75.

- Guo, XY, XM Liu, L Jin, TT Wang, K Ullah, JZ Sheng, and HF Huang** 2017 Cardiovascular and metabolic profiles of offspring conceived by assisted reproductive technologies: a systematic review and meta-analysis. *Fertil Steril* **107** 622-631 e625.
- Halliwell, B, and CY Lee** 2010 Using isoprostanes as biomarkers of oxidative stress: some rarely considered issues. *Antioxid Redox Signal* **13** 145-156.
- Henderson, GC, MA Horning, SL Lehman, EE Wolfel, BC Bergman, and GA Brooks** 2004 Pyruvate shuttling during rest and exercise before and after endurance training in men. *J Appl Physiol* **97** 317-325.
- Johnson, MH, and MH Nasr-Esfahani** 1994 Radical solutions and cultural problems: could free oxygen radicals be responsible for the impaired development of preimplantation mammalian embryos in vitro? *Bioessays* **16** 31-38.
- Keller, RJ, NC Halmes, JA Hinson, and NR Pumford** 1993 Immunochemical detection of oxidized proteins. *Chem Res Toxicol* **6** 430-433.
- Kleijkers, SH, E Mantikou, E Slappendel, D Consten, J van Echten-Arends, AM Wetzels, M van Wely, LJ Smits, AP van Montfoort, S Repping, JC Dumoulin, and S Mastenbroek** 2016 Influence of embryo culture medium (G5 and HTF) on pregnancy and perinatal outcome after IVF: a multicenter RCT. *Hum Reprod* **31** 2219-2230.
- Kleijkers, SH, AP van Montfoort, LJ Smits, W Viechtbauer, TJ Roseboom, EC Nelissen, E Coonen, JG Derhaag, L Bastings, IE Schreurs, JL Evers, and JC Dumoulin** 2014 IVF culture medium affects post-natal weight in humans during the first 2 years of life. *Hum Reprod* **29** 661-669.
- Lane, M, and DK Gardner** 1996 Selection of viable mouse blastocysts prior to transfer using a metabolic criterion. *Hum Reprod* **11** 1975-1978.
- Lane, M, and DK Gardner** 1998 Amino acids and vitamins prevent culture-induced metabolic perturbations and associated loss of viability of mouse blastocysts. *Hum Reprod* **13** 991-997.
- Lane, M, and DK Gardner** 2000 Lactate regulates pyruvate uptake and metabolism in the preimplantation mouse embryo. *Biol Reprod* **62** 16-22.
- Leese, HJ** 2012 Metabolism of the preimplantation embryo: 40 years on. *Reproduction* **143** 417-427.
- Leese, HJ, F Guerif, V Allgar, DR Brison, K Lundin, and RG Sturmey** 2016 Biological optimization, the Goldilocks principle, and how much is lagom in the preimplantation embryo. *Mol Reprod Dev* **83** 748-754.
- Li, SS, YH Liu, CN Tseng, and S Singh** 2006 Analysis of gene expression in single human oocytes and preimplantation embryos. *Biochem Biophys Res Commun* **340** 48-53.
- Liu, C, J Wu, J Zhu, C Kuei, J Yu, J Shelton, SW Sutton, X Li, SJ Yun, T Mirzadegan, C Mazur, F Kamme, and TW Lovenberg** 2009 Lactate inhibits lipolysis in fat cells through activation of an orphan G-protein-coupled receptor, GPR81. *J Biol Chem* **284** 2811-2822.
- Luo, W, and C Brouwer** 2013 Pathview: an R/Bioconductor package for pathway-based data integration and visualization. *Bioinformatics* **29** 1830-1831.
- Luvoni, GC, L Keskinetepe, and BG Brackett** 1996 Improvement in bovine embryo production in vitro by glutathione-containing culture media. *Mol Reprod Dev* **43** 437-443.
- Ma, YY, HW Chen, and CR Tzeng** 2017 Low oxygen tension increases mitochondrial membrane potential and enhances expression of antioxidant genes and implantation protein of mouse blastocyst cultured in vitro. *J Ovarian Res* **10** 47.
- Marei, WFA, L Van den Bosch, I Pintelon, O Mohey-Elsaeed, PEJ Bols, and J Leroy** 2019 Mitochondria-targeted therapy rescues development and quality of embryos derived from oocytes matured under oxidative stress conditions: a bovine in vitro model. *Hum Reprod* **34** 1984-1998.
- Markert, CL, JB Shaklee, and GS Whitt** 1975 Evolution of a gene. Multiple genes for LDH isozymes provide a model of the evolution of gene structure, function and regulation. *Science* **189** 102-114.

- Martin-Romero, FJ, EM Miguel-Lasobras, JA Dominguez-Arroyo, E Gonzalez-Carrera, and IS Alvarez** 2008 Contribution of culture media to oxidative stress and its effect on human oocytes. *Reprod Biomed Online* **17** 652-661.
- McKinney, ET, R Shouri, RS Hunt, RA Ahokas, and BM Sibai** 2000 Plasma, urinary, and salivary 8-epi-prostaglandin f2alpha levels in normotensive and preeclamptic pregnancies. *Am J Obstet Gynecol* **183** 874-877.
- Meintjes, M, SJ Chantilis, JD Douglas, AJ Rodriguez, AR Guerami, DM Bookout, BD Barnett, and JD Madden** 2009 A controlled randomized trial evaluating the effect of lowered incubator oxygen tension on live births in a predominantly blastocyst transfer program. *Hum Reprod* **24** 300-307.
- Meister, TA, SF Rimoldi, R Soria, R von Arx, FH Messerli, C Sartori, U Scherrer, and E Rexhaj** 2018 Association of Assisted Reproductive Technologies With Arterial Hypertension During Adolescence. *J Am Coll Cardiol* **72** 1267-1274.
- Montuschi, P, E Ragazzoni, S Valente, G Corbo, C Mondino, G Ciappi, and G Ciabattoni** 2003 Validation of 8-isoprostane and prostaglandin E(2) measurements in exhaled breath condensate. *Inflamm Res* **52** 502-507.
- Nishihara, T, K Matsumoto, Y Hosoi, and Y Morimoto** 2018 Evaluation of antioxidant status and oxidative stress markers in follicular fluid for human in vitro fertilization outcome. *Reprod Med Biol* **17** 481-486.
- Parks, SK, J Chiche, and J Pouyssegur** 2011 pH control mechanisms of tumor survival and growth. *J Cell Physiol* **226** 299-308.
- Preis, KA, GE Seidel, Jr., and DK Gardner** 2007 Reduced oxygen concentration improves the developmental competence of mouse oocytes following in vitro maturation. *Mol Reprod Dev* **74** 893-903.
- Psathakis, K, G Papatheodorou, M Plataki, P Panagou, S Loukides, NM Sifakas, and D Bouros** 2004 8-Isoprostane, a marker of oxidative stress, is increased in the expired breath condensate of patients with pulmonary sarcoidosis. *Chest* **125** 1005-1011.
- Qin, JB, XQ Sheng, D Wu, SY Gao, YP You, TB Yang, and H Wang** 2017 Worldwide prevalence of adverse pregnancy outcomes among singleton pregnancies after in vitro fertilization/intracytoplasmic sperm injection: a systematic review and meta-analysis. *Arch Gynecol Obstet* **295** 285-301.
- Redel, BK, AN Brown, LD Spate, KM Whitworth, JA Green, and RS Prather** 2011 Glycolysis in preimplantation development is partially controlled by the Warburg Effect. *Mol Reprod Dev.*
- Reik, W** 2007 Stability and flexibility of epigenetic gene regulation in mammalian development. *Nature* **447** 425-432.
- Reik, W, W Dean, and J Walter** 2001 Epigenetic reprogramming in mammalian development. *Science* **293** 1089-1093.
- Ren, L, Z Wang, L An, Z Zhang, K Tan, K Miao, L Tao, L Cheng, Z Zhang, M Yang, Z Wu, and J Tian** 2015 Dynamic comparisons of high-resolution expression profiles highlighting mitochondria-related genes between in vivo and in vitro fertilized early mouse embryos. *Human Reproduction* **dev** **228**.
- Rinaudo, P, G Giritharan, S Talbi, A Dobson, and R Schultz** 2006a Effects of oxygen tension on gene expression in preimplantation mouse embryos. *Fertility and Sterility* **86** 1265.e1261-1265.e1236.
- Rinaudo, P, and RM Schultz** 2004 Effects of embryo culture on global pattern of gene expression in preimplantation mouse embryos. *Reproduction* **128** 301-311.
- Rinaudo, PF, G Giritharan, S Talbi, AT Dobson, and RM Schultz** 2006b Effects of oxygen tension on gene expression in preimplantation mouse embryos. *Fertil Steril* **86** 1252-1265, 1265 e1251-1236.
- Rizzo, A, MT Roscino, F Binetti, and RL Sciorsci** 2012 Roles of reactive oxygen species in female reproduction. *Reprod Domest Anim* **47** 344-352.
- Rogatzki, MJ, BS Ferguson, ML Goodwin, and LB Gladden** 2015 Lactate is always the end product of glycolysis. *Front Neurosci* **9** 22.

- Ruggeri, E, S Lira-Albarran, EJ Grow, X Liu, R Harner, E Maltepe, M Ramalho-Santos, A Donjacour, and P Rinaudo** 2020 Sex-Specific Epigenetic Profile of Inner Cell Mass of Mice Conceived In Vivo or by In-Vitro Fertilization. *Mol Hum Reprod*.
- Ryan, HE, J Lo, and RS Johnson** 1998 HIF-1 alpha is required for solid tumor formation and embryonic vascularization. *EMBO J* **17** 3005-3015.
- Shibata, S, S Sogabe, M Miwa, T Fujimoto, N Takakura, A Naotsuka, S Kitamura, T Kawamoto, and T Soga** 2021 Identification of the first highly selective inhibitor of human lactate dehydrogenase B. *Sci Rep* **11** 21353.
- Summermatter, S, G Santos, J Perez-Schindler, and C Handschin** 2013 Skeletal muscle PGC-1alpha controls whole-body lactate homeostasis through estrogen-related receptor alpha-dependent activation of LDH B and repression of LDH A. *Proc Natl Acad Sci U S A* **110** 8738-8743.
- Takahashi, M, T Nagai, S Hamano, M Kuwayama, N Okamura, and A Okano** 1993 Effect of thiol compounds on in vitro development and intracellular glutathione content of bovine embryos. *Biol Reprod* **49** 228-232.
- Tzika, E, T Dreker, and A Imhof** 2018 Epigenetics and Metabolism in Health and Disease. *Front Genet* **9** 361.
- Van Blerkom, J** 2011 Mitochondrial function in the human oocyte and embryo and their role in developmental competence. *Mitochondrion* **11** 797-813.
- Waldenstrom, U, AB Engstrom, D Hellberg, and S Nilsson** 2009 Low-oxygen compared with high-oxygen atmosphere in blastocyst culture, a prospective randomized study. *Fertil Steril* **91** 2461-2465.
- Warburg, O** 1956 On the origin of cancer cells. *Science* **123** 309-314.
- Webb, BA, M Chimenti, MP Jacobson, and DL Barber** 2011 Dysregulated pH: a perfect storm for cancer progression. *Nat Rev Cancer* **11** 671-677.
- Xiao Z, Donjacour A, Harner R, Rhodel S, Kao C-N, Ruggeri E., Liu X, Maltepe E., and R P** 2020 Effect of culture conditions and method of conception on mouse live birth rate. *Fertil Steril Sci* **1** 132-141.
- Yamaguchi, S, and J Yoshino** 2017 Adipose tissue NAD(+) biology in obesity and insulin resistance: From mechanism to therapy. *Bioessays* **39**.
- Yang, W, P Wang, P Cao, S Wang, Y Yang, H Su, and B Nashun** 2021 Hypoxic in vitro culture reduces histone lactylation and impairs pre-implantation embryonic development in mice. *Epigenetics Chromatin* **14** 57.
- Yang, Y, and AA Sauve** 2016 NAD(+) metabolism: Bioenergetics, signaling and manipulation for therapy. *Biochim Biophys Acta* **1864** 1787-1800.